**Table 21.4 Pressure–Viscosity Coefficients for Test Fluids at Three Temperatures (From Ref. 17)**

| | Temperature, °C | | |
|---|---|---|---|
| | 38 | 99 | 149 |
| Test Fluid | Pressure-viscosity Coefficient, $\xi$, m²/N | | |
| Advanced ester | $1.28 \times 10^{-8}$ | $0.987 \times 10^{-8}$ | $0.851 \times 10^{-8}$ |
| Formulated advanced ester | 1.37 | 1.00 | .874 |
| Polyalkyl aromatic | 1.58 | 1.25 | 1.01 |
| Polyalkyl aromatic + 10 wt % heavy resin | 1.70 | 1.28 | 1.06 |
| Synthetic paraffinic oil (lot 3) | 1.77 | 1.51 | 1.09 |
| Synthetic paraffinic oil (lot 4) | 1.99 | 1.51 | 1.29 |
| Synthetic paraffinic oil (lot 4) + antiwear additive | 1.96 | 1.55 | 1.25 |
| Synthetic paraffinic oil (lot 2) + antiwear additive | 1.81 | 1.37 | 1.13 |
| C-ether | 1.80 | .980 | .795 |
| Superrefined naphthenic mineral oil | 2.51 | 1.54 | 1.27 |
| Synthetic hydrocarbon (traction fluid) | 3.12 | 1.71 | .939 |
| Fluorinated polyether | 4.17 | 3.24 | 3.02 |

$$\delta(x,y) = \frac{2}{\pi E'} \iint_\Lambda \frac{p(x,y)\,dx_1 dy_1}{[(x - x_1)^2 + (y - y_1)^2]^{1/2}} \qquad (21.11)$$

where

$$E' = 2 \left( \frac{1 - \nu_a^2}{E_a} + \frac{1 - \nu_b^2}{E_b} \right)^{-1} \qquad (21.12)$$

and $\nu$ = Poisson's ratio
$E$ = modulus of elasticity, N/m²

Therefore, Eq. (21.6) is normally involved in hydrodynamic lubrication situations, while Eqs. (21.7)–(21.11) are normally involved in elastohydrodynamic lubrication situations.

## 21.2 HYDRODYNAMIC AND HYDROSTATIC LUBRICATION

Surfaces lubricated hydrodynamically are normally conformal as pointed out in Section 21.1.1. The conformal nature of the surfaces can take its form either as a thrust bearing or as a journal bearing, both of which will be considered in this section. Three features must exist for hydrodynamic lubrication to occur:

1. A viscous fluid must separate the lubricated surfaces.
2. There must be relative motion between the surfaces.
3. The geometry of the film shape must be larger in the inlet than at the outlet so that a convergent wedge of lubricant is formed.

If feature 2 is absent, lubrication can still be achieved by establishing relative motion between the fluid and the surfaces through external pressurization. This is discussed further in Section 21.2.3.

In hydrodynamic lubrication the entire friction arises from the shearing of the lubricant film so that it is determined by the viscosity of the oil: the thinner (or less viscous) the oil, the lower the friction. The great advantages of hydrodynamic lubrication are that the friction can be very low ($\mu \simeq 0.001$) and, in the ideal case, there is no wear of the moving parts. The main problems in hydrodynamic lubrication are associated with starting or stopping since the oil film thickness theoretically is zero when the speed is zero.

The emphasis in this section is on hydrodynamic and hydrostatic lubrication. This section is not intended to be all inclusive but rather to typify the situations existing in hydrodynamic and hydrostatic lubrication. For additional information the reader is recommended to investigate Gross et al.,[19] Reiger,[20] Pinkus and Sternlicht,[21] and Rippel.[22]

### 21.2.1   Liquid-Lubricated Hydrodynamic Journal Bearings

Journal bearings, as shown in Fig. 21.8, are used to support shafts and to carry radial loads with minimum power loss and minimum wear. The bearing can be represented by a plain cylindrical bush wrapped around the shaft, but practical bearings can adopt a variety of forms. The lubricant is supplied at some convenient point through a hole or a groove. If the bearing extends around the full 360° of the shaft, the bearing is described as a full journal bearing. If the angle of wrap is less than 360°, the term "partial journal bearing" is employed.

**Plain**

Journal bearings rely on the motion of the shaft to generate the load-supporting pressures in the lubricant film. The shaft does not normally run concentric with the bearing center. The distance between the shaft center and the bearing center is known as the eccentricity. This eccentric position within the bearing clearance is influenced by the load that it carries. The amount of eccentricity adjusts itself until the load is balanced by the pressure generated in the converging portion of the bearing. The pressure generated, and therefore the load capacity of the bearing, depends on the shaft eccentricity $e$, the frequency of rotation $N$, and the effective viscosity of the lubricant $\eta$ in the converging film, as well as the bearing dimensions $l$ and $d$ and the clearance $c$. The three dimensionless groupings normally used for journal bearings are:

1. The eccentricity ratio, $\epsilon = e/c$
2. The length-to-diameter ratio, $\lambda = l/d$
3. The Sommerfeld number, $Sm = \eta N d^3 l / 2Fc^2$

When designing a journal bearing, the first requirement to be met is that it should operate with an adequate minimum film thickness, which is directly related to the eccentricity ($h_{min} = c - e$). Figures 21.9, 21.10, and 21.11 show the eccentricity ratio, the dimensionless minimum film thickness, and the dimensionless Sommerfeld number for, respectively, a full journal bearing and partial journal bearings of 180° and 120°. In these figures a recommended operating eccentricity ratio is indicated as well as a preferred operational area. The left boundary of the shaded zone defines the optimum eccentricity ratio for minimum coefficient of friction, and the right boundary is the optimum eccentricity ratio for maximum load. In these figures it can be observed that the shaded area is significantly reduced for the partial bearings as compared with the full journal bearing. These plots were adapted from results given in Raimondi and Boyd.[23]

Figures 21.12, 21.13, and 21.14 show a plot of attitude angle $\phi$ (angle between the direction of the load and a line drawn through the centers of the bearing and the journal) and the bearing characteristic number for various length-to-diameter ratios for, respectively, a full journal bearing and partial journal bearings of 180° and 120°. This angle establishes where the minimum and maximum film thicknesses are located within the bearing. These plots were also adapted from results given in Raimondi and Boyd,[23] where additional information about the coefficient of friction, the flow variable, the temperature rise, and the maximum film pressure ratio for a complete range of length-to-diameter ratios as well as for full or partial journal bearings can be found.
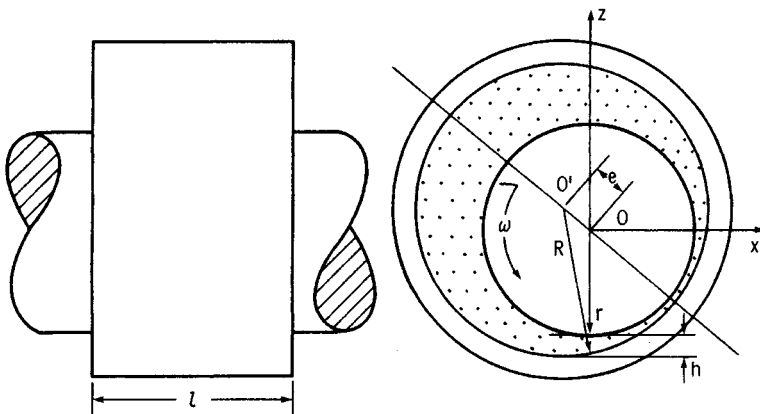


**Fig. 21.8**   Journal bearing.
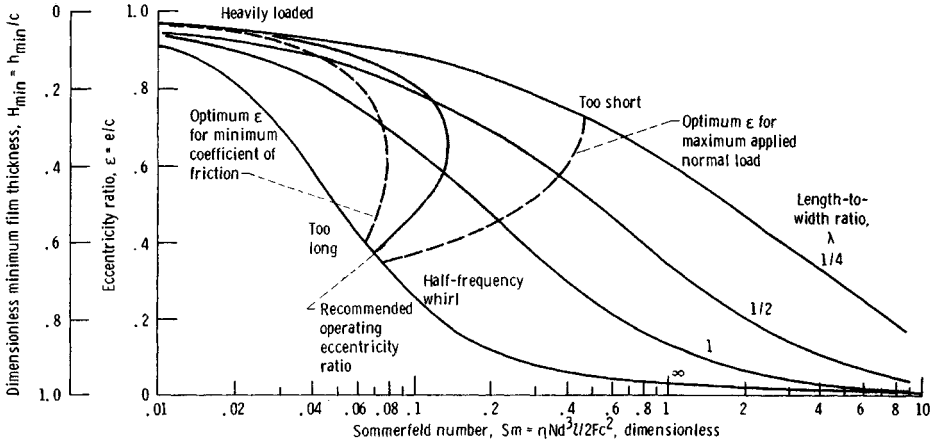
**Fig. 21.9** Design figure showing eccentricity ratio, dimensionless minimum film thickness, and Sommerfeld number for full journal bearings. (Adapted from Ref. 23.)

### Nonplain

As applications have demanded higher speeds, vibration problems due to critical speeds, imbalance, and instability have created a need for journal bearing geometries other than plain journal bearings. These geometries have various patterns of variable clearance so as to create pad film thicknesses that have more strongly converging and diverging regions. Figure 21.15 shows elliptical, offset half, three-lobe, and four-lobe bearings—bearings different from the plain journal bearing. An excellent discussion of the performance of these bearings is provided in Allaire and Flack,[24] and some of their conclusions are presented here. In Fig. 21.15, each pad is moved in toward the center of the bearing some fraction of the pad clearance in order to make the fluid-film thickness more converging and diverging than that which occurs in a plain journal bearing. The pad center of curvature is indicated by a cross. Generally, these bearings give good suppression of instabilities in the system but can be subject to subsynchronous vibration at high speeds. Accurate manufacturing of these bearings is not always easy to obtain.
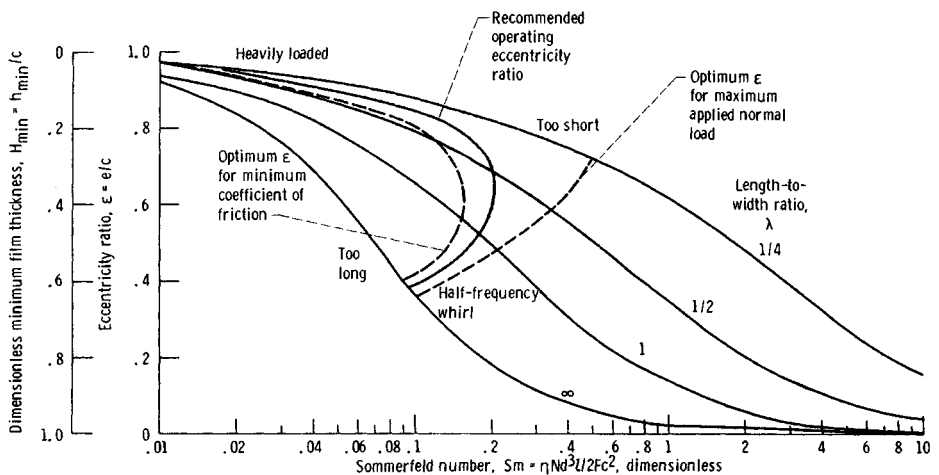


**Fig. 21.10** Design figure showing eccentricity ratio, dimensionless minimum film thickness, and Sommerfeld number for 180° partial journal bearings, centrally loaded. (Adapted from Ref. 23.)
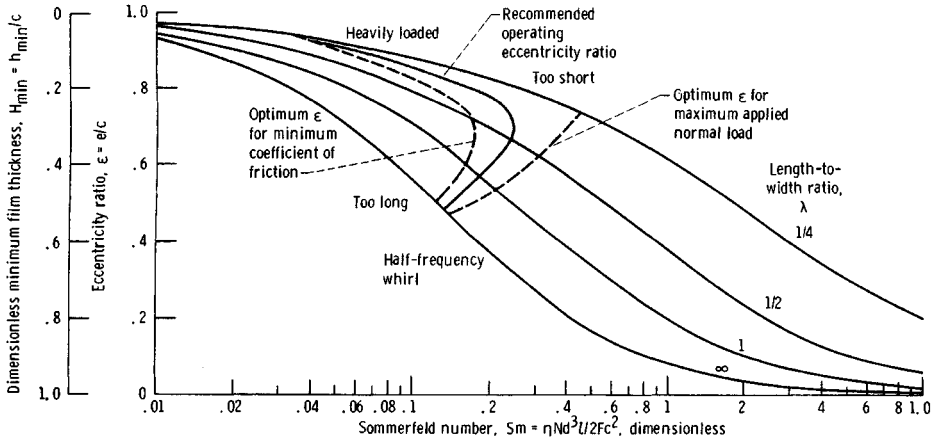
**Fig. 21.11**  Design figure showing eccentricity ratio, dimensionless minimum film thickness, and Sommerfeld number for 120° partial journal bearings, centrally loaded. (Adapted from Ref. 23.)
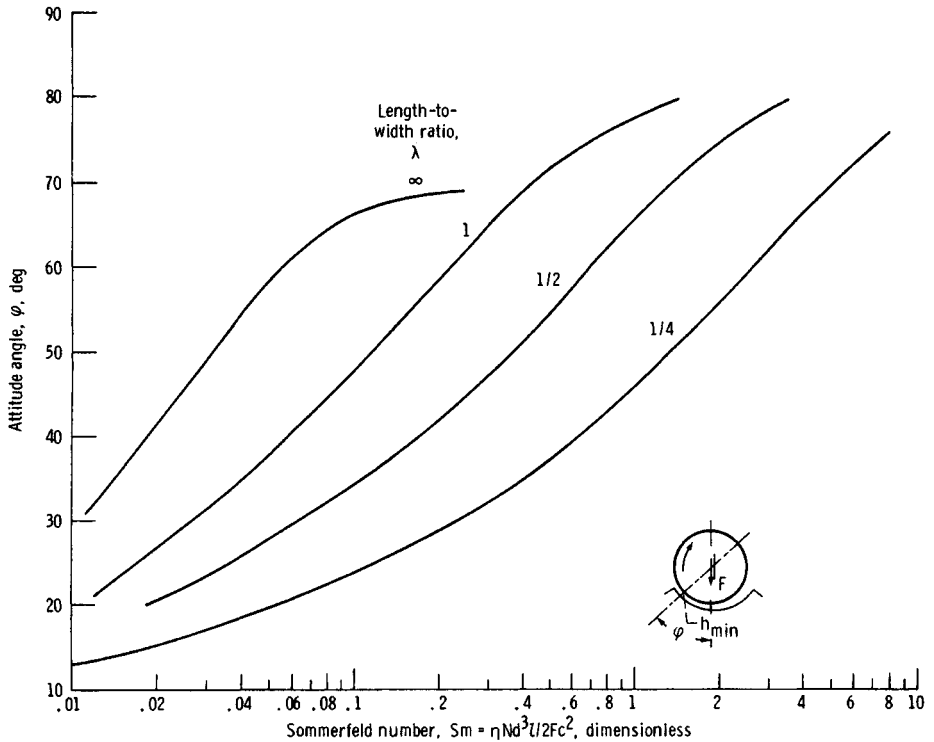


**Fig. 21.12**  Design figure showing attitude angle (position of minimum film thickness) and Sommerfeld number for full journal bearings, centrally loaded. (Adapted from Ref. 23.)
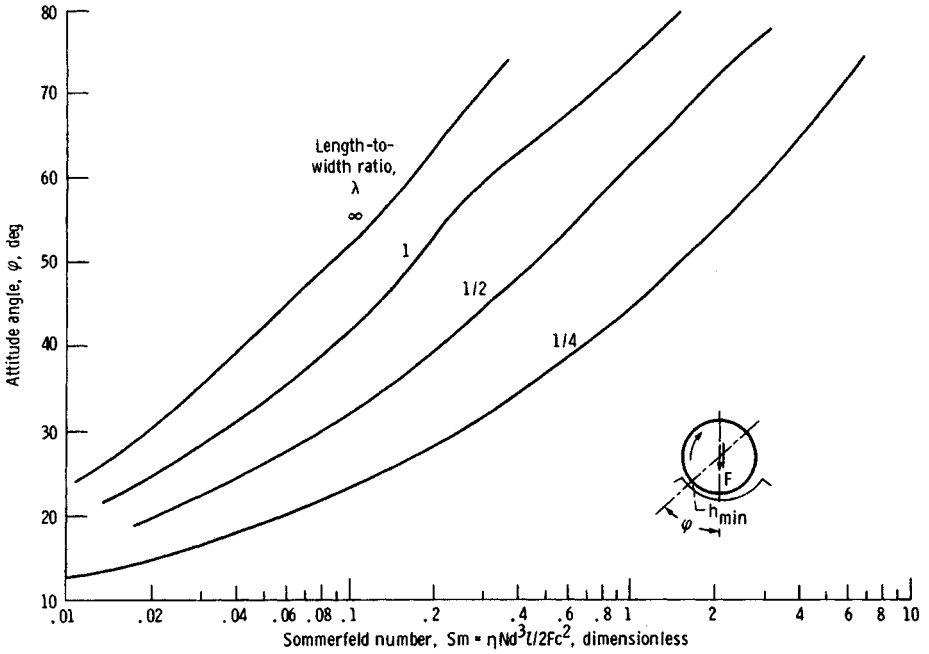
**Fig. 21.13** Design figure showing attitude angle (position of minimum film thickness) and Sommerfeld number for 180° partial journal bearings, centrally loaded. (Adapted from Ref. 23.)
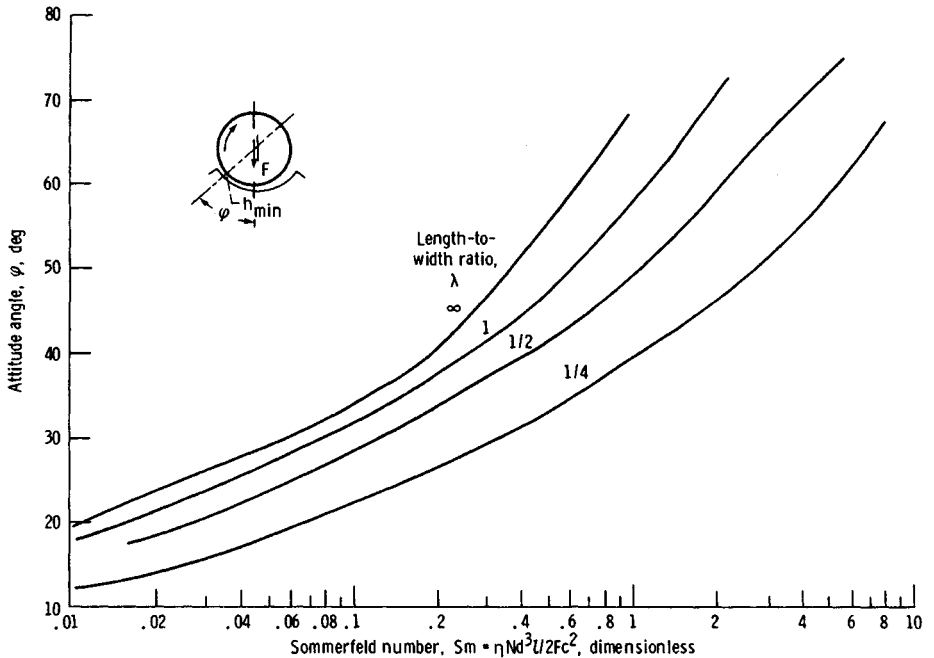


**Fig. 21.14** Design figure showing attitude angle (position of minimum film thickness) and Sommerfeld number for 120° partial journal bearings, centrally loaded. (Adapted from Ref. 23.)
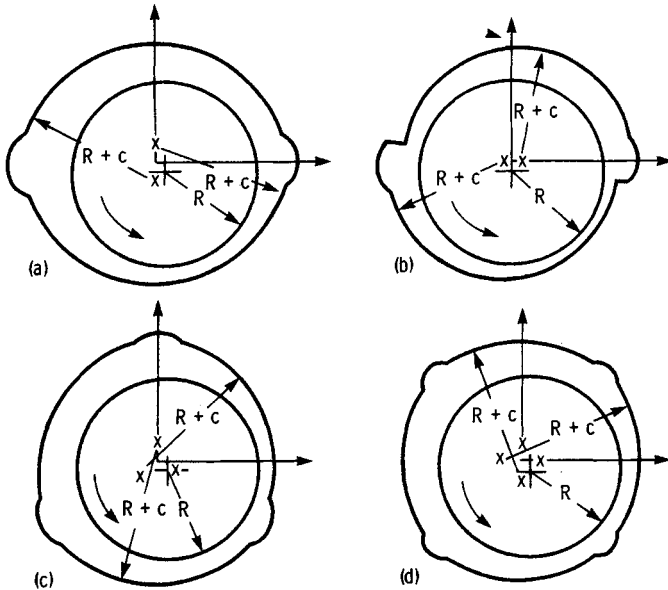
**Fig. 21.15**  Types of fixed-incline pad preloaded journal bearings. (From Ref. 24.) (a) Elliptical bore bearing ($\alpha_a = 0.5$, $m_p = 0.4$). (b) Offset half bearing ($\alpha_a = 1.125$, $m_p = 0.4$). (c) Three-lobe bearing ($\alpha_a = 0.5$, $m_p = 0.4$). (d) Four-lobe bearing ($\alpha_a = 0.5$, $m_p = 0.4$).

A key parameter used in describing these bearings is the fraction of length in which the film thickness is converging to the full pad length, called the offset factor and defined as

$$\alpha_a = \frac{\text{length of pad with converging film thickness}}{\text{full pad length}}$$

The elliptical bearing, shown in Fig. 21.15, indicates that the two pad centers of curvature are moved along the $y$ axis. This creates a pad with one-half of the film shape converging and the other half diverging (if the shaft were centered), corresponding to an offset factor $\alpha_a = 0.5$. The offset half bearing in Fig. 21.15$b$ consists of a two-axial-groove bearing that is split by moving the top half horizontally. This results in low vertical stiffness.

Generally, the vibration characteristics of this bearing are such as to avoid the previously mentioned oil whirl, which can drive a machine unstable. The offset half bearing has a purely converging film thickness with a converged pad arc length of 160° and the point opposite the center of curvature at 180°. Both the three-lobe and four-lobe bearings shown in Figs. 21.15$c$ and 21.15$d$ have an offset factor of $\alpha_a = 0.5$.

The fractional reduction of the film clearance when the pads are brought in is called the preload factor $m_p$. Let the bearing clearance at the pad minimum film thickness (with the shaft center) be denoted by $c_b$. Figure 21.16$a$ shows that the largest shaft that can be placed in the bearing has a radius $R + c_b$, thereby establishing the definition of $c_b$. The preload factor $m_p$ is given by

$$m_p = \frac{c - c_b}{c}$$

A preload factor of zero corresponds to having all of the pad centers of curvature coinciding at the center of the bearing; a preload factor of 1.0 corresponds to having all of the pads touching the shaft. Figures 21.16$b$ and 21.16$c$ illustrate these extreme situations. Values of the preload factor are indicated in the various types of fixed journal bearings shown in Fig. 21.15.

Figure 21.17 shows the variation of the whirl ratio with Sommerfeld number at the threshold of instability for the four bearing types shown in Fig. 21.15. It is evident that a definite relationship exists between the stability and whirl ratio such that the more stable bearing distinctly whirls at a lower speed ratio. With the exception of the elliptical bearing, all bearings whirl at speeds less than
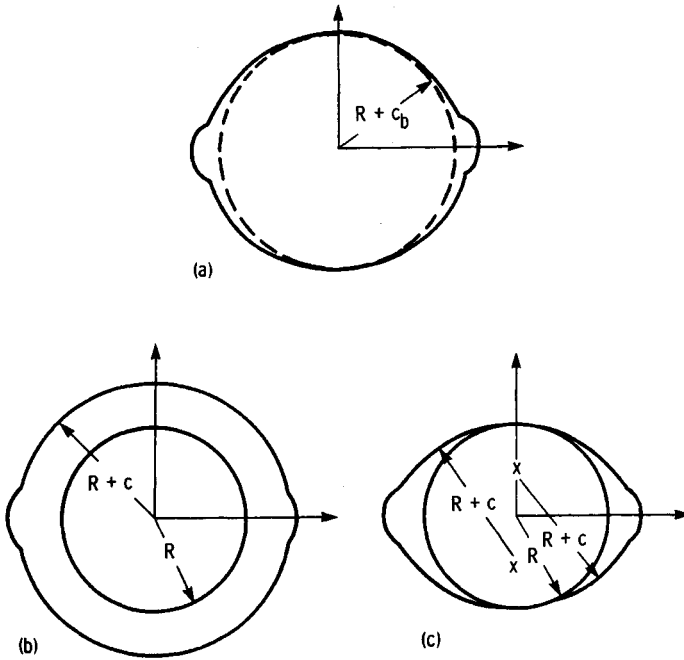
**Fig. 21.16** Effect of preload on two-lobe bearings. (From Ref. 24.) (a) Largest shaft that fits in bearing. (b) $m = 0$, largest shaft $= R + c$, bearing clearance $c_b = $ (c). (c) $m = 1.0$, largest shaft $= R$, bearing clearance $c_b = 0$.
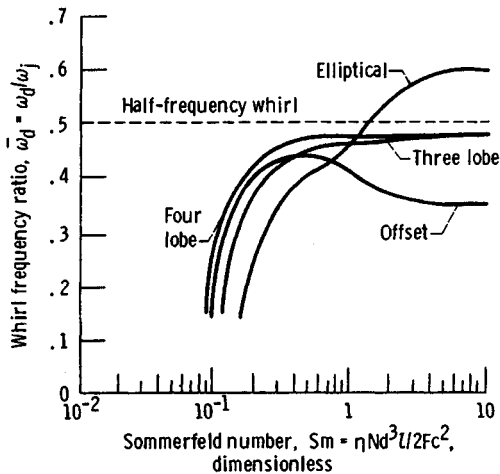


**Fig. 21.17** Chart for determining whirl frequency ratio. (From Ref. 24.)

0.48 of the rotor speed. The offset bearing attains a maximum whirl ratio of 0.44 at a Sommerfeld number of about 0.4 and decreases to a steady value of 0.35 at higher Sommerfeld numbers. This observation corresponds to the superior stability with the offset bearing at high-speed and light-load operations.

The whirl ratios with the three-lobe and four-lobe bearings share similar characteristics. They both rise sharply at low Sommerfeld numbers and remain fairly constant for most portions of the curves. Asymptotic whirl ratios of 0.47 and 0.48, respectively, are reached at high Sommerfeld numbers. In comparison with the four-lobe bearing, the three-lobe bearing always has the lower whirl ratio.

The elliptical bearing is the least desirable for large Sommerfeld numbers. At $Sm > 1.3$ the ratio exceeds 0.5.

### 21.2.2   Liquid-Lubricated Hydrodynamic Thrust Bearings

In a thrust bearing, a thrust plate attached to, or forming part of, the rotating shaft is separated from the sector-shaped bearing pads by a film of lubricant. The load capacity of the bearing arises entirely from the pressure generated by the motion of the thrust plate over the bearing pads. This action is achieved only if the clearance space between the stationary and moving components is convergent in the direction of motion. The pressure generated in, and therefore the load capacity of, the bearing, depends on the velocity of the moving slider $u = (R_1 + R_2)\omega/2 = \pi(R_1 + R_2)N$, the effective viscosity, the length of the pad $l$, the width of the pad $b$, the normal applied load $F$, the inlet film thickness $h_i$, and the outlet film thickness $h_0$. For thrust bearings three dimensionless parameters are used:

1. $\lambda = l/b$, pad length-to-width ratio
2. $Sm_t = \eta u b l^2 / F h_o^2$, Sommerfeld number for thrust bearings
3. $\bar{h}_i = h_i/h_o$, film thickness ratio

It is important to recognize that the total thrust load $F$ is equal to $nF$, where $n$ is the number of pads in a thrust bearing. In this section three different thrust bearings will be investigated. Two fixed-pad types, a fixed incline and a step sector, and a pivoted-pad type will be discussed.

#### Fixed-Incline Pad

The simplest form of fixed-pad thrust bearing provides only straight-line motion and consists of a flat surface sliding over a fixed pad or land having a profile similar to that shown in Fig. 21.18. The fixed-pad bearing depends for its operation on the lubricant being drawn into a wedge-shaped space
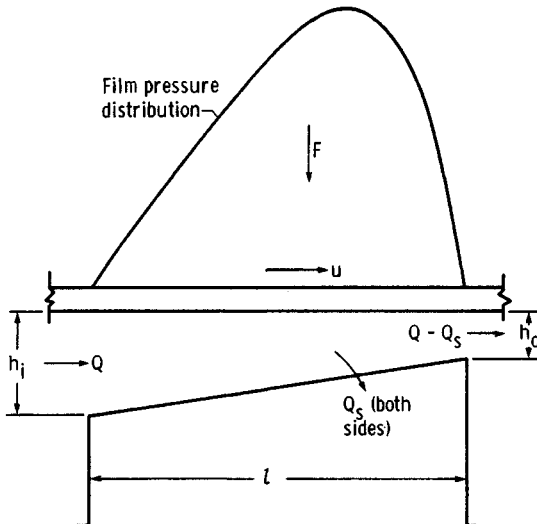


**Fig. 21.18**   Configuration of fixed-incline pad bearing. (From Ref. 25. Reprinted by permission of ASME.)
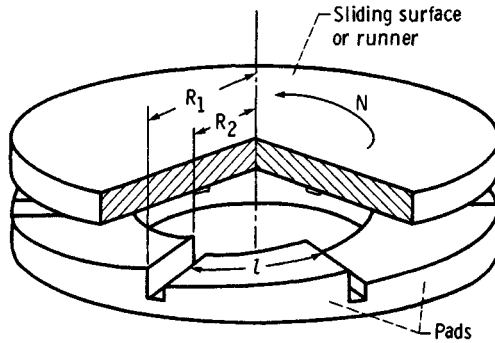
**Fig. 21.19** Configuration of fixed-incline pad thrust bearing. (From Ref. 25.)

and thus producing pressure that counteracts the load and prevents contact between the sliding parts. Since the wedge action only takes place when the sliding surface moves in the direction in which the lubricant film converges, the fixed-incline bearing, shown in Fig. 21.18, can only carry load for this direction of operation. If reversibility is desired, a combination of two or more pads with their surfaces sloped in opposite direction is required. Fixed-incline pads are used in multiples as in the thrust bearing shown in Fig. 21.19.

The following procedure assists in the design of a fixed-incline pad thrust bearing:

1. Choose a pad width-to-length ratio. A square pad ($\lambda = 1$) is generally felt to give good performance. From Fig. 21.20, if it is known whether maximum load or minimum power is most important in the particular application, a value of the film thickness ratio can be determined.
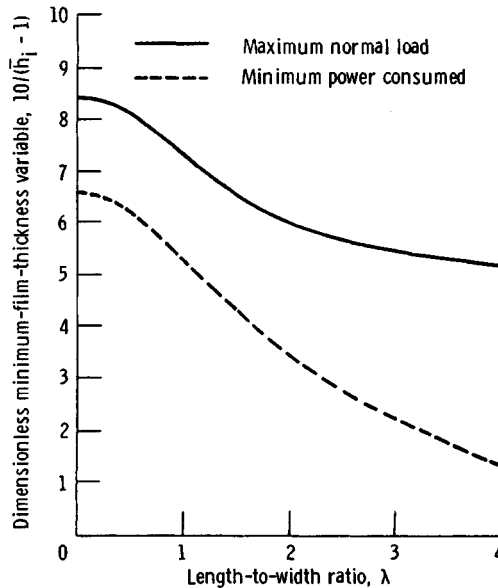


**Fig. 21.20** Chart for determining minimum film thickness corresponding to maximum load or minimum power less for various pad proportions—fixed-incline pad bearings. (From Ref. 25. Reprinted by permission of ASME.)

2. Within the terms in the Sommerfeld number the term least likely to be preassigned is the outlet film thickness. Therefore, determine $h_o$ from Fig. 21.21. Since $\bar{h}_i$ is known from Fig. 21.20, $h_i$ can be determined ($h_i = \bar{h}_i h_o$).

3. Check Table 21.5 to see if minimum (outlet) film thickness is sufficient for the preassigned surface finish. If not:

   a. Increase the fluid viscosity or speed of the bearing.

   b. Decrease the load or the surface finish. Upon making this change return to step 1.

4. Once an adequate minimum film thickness has been determined, use Figs. 21.22–21.24 to obtain, respectively, the coefficient of friction, the power consumed, and the flow.

## Pivoted Pad

The simplest form of pivoted-pad bearing provides only for straight-line motion and consists of a flat surface sliding over a pivoted pad as shown in Fig. 21.25. If the pad is assumed to be in equilibrium under a given set of operating conditions, any change in these conditions, such as a change in load, speed, or viscosity, will alter the pressure distribution and thus momentarily shift the center of pressure and create a moment that causes the pad to change its inclination until a new position of equilibrium is established. It can be shown that if the position of that pivot, as defined by the distance $\bar{x}$, is fixed by choosing $\bar{x}/l$, the ratio of the inlet film thickness to the outlet film thickness, $h_i/h_o$, also becomes fixed and is independent of load, speed, and viscosity. Thus the pad will automatically alter its inclination so as to maintain a constant value of $h_i/h_o$.

Pivoted pads are sometimes used in multiples as pivoted-pad thrust bearings, shown in Fig. 21.26. Calculations are carried through for a single pad, and the properties for the complete bearing are found by combining these calculations in the proper manner.

Normally, a pivoted pad, will only carry load if the pivot is placed somewhere between the center of the pad and the outlet edge ($0.5 < \bar{x}/l \leq 1.0$). With the pivot so placed, the pad therefore can only carry load for one direction of rotation.

The following procedure helps in the design of pivoted-pad thrust bearings:

1. Having established if minimum power or maximum load is more critical in the particular application and chosen a pad length-to-width ratio, establish the pivot position from Fig. 21.27.

2. In the Sommerfeld number for thrust bearings the unknown parameter is usually the outlet or minimum film thickness. Therefore, establish the value of $h_o$ from Fig. 21.28.

3. Check Table 21.5 to see if the outlet film thickness is sufficient for the preassigned surface finish. If sufficient, go on to step 4. If not, consider:

   a. Increasing the fluid viscosity

   b. Increasing the speed of the bearing

   c. Decreasing the load of the bearing

   d. Decreasing the surface finish of the bearing lubrication surfaces
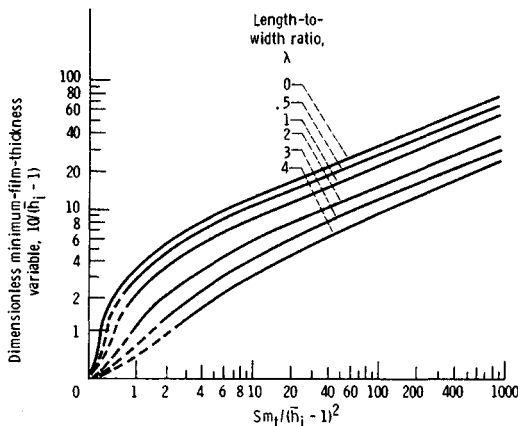


**Fig. 21.21**   Chart for determining minimum film thickness for fixed-incline pad thrust bearings. (From Ref. 25. Reprinted by permission of ASME.)

**Table 21.5 Allowable Minimum Outlet Film Thickness for a Given Surface Finish (From Ref. 8)**

| Surface Finish | | | | | Allowable Minimum Outlet Film Thickness[a], $h_0$ | |
|---|---|---|---|---|---|---|
| Familiar British Units, $\mu$in, CLA[b] | SI Units, $\mu$in[c] CLA | Description of Surface | Examples of Manufacturing Methods | Approximate Relative Costs | Familiar British Units, in. | SI Units, m |
| 4–8 | 0.1–0.2 | Mirror-like surface without toolmarks, close tolerances | Grind, lap, and superfinish | 17–20 | 0.00010 | 0.0000025 |
| 8–16 | 0.2–0.4 | Smooth surface without scratches, close tolerances | Grind and lap | 17–20 | .00025 | .0000062 |
| 16–32 | 0.4–0.8 | Smooth surface, close tolerances | Grind, file, and lap | 10 | .00050 | .0000125 |
| 32–63 | 0.8–1.6 | Accurate bearing surface without toolmarks | Grind, precision mill, and file | 7 | .00100 | .000025 |
| 63–125 | 1.6–3.2 | Smooth surface without objectionable toolmarks, moderate tolerances | Shape, mill, grind, and turn | 5 | .00200 | .000050 |

[a]The values of film thickness are given only for guidance. They indicate the film thickness required to avoid metal-to-metal contact under clean oil conditions with no misalignment. It may be necessary to take a larger film thickness than that indicated (e.g., to obtain an acceptable temperature rise). It has been assumed that the average surface finish of the pads is the same as that of the runner.

[b]CLA = centerline average.

[c]$\mu$m = micrometer; 40 $\mu$in. (microinch) = 1 $\mu$m.

Upon making this change return to step 1.

**4.** Once an adequate outlet film thickness is established, determine the film thickness ratio, power loss, coefficient of friction, and flow from Figs. 21.29–21.32.

## Step Sector

The configuration of a step-sector thrust bearing is shown in Fig. 21.33. The parameters used to define the dimensionless load and stiffness are:

**1.** $\bar{h}_i = h_i/h_o$, film thickness ratio.
**2.** $\bar{\theta} = \theta_i/(\theta_i + \theta_o)$, dimensionless step location.
**3.** $n$, number of sectors.
**4.** $\alpha_r = R_2 R_1$, radius ratio.
**5.** $\theta_g$, angular extent of lubrication feed groove.

Note that the first four parameters are dimensionless and the fifth is dimensional and expressed in radians.

The optimum parallel step-sector bearing for *maximum load capacity* for a given $\alpha_r$ and $\theta_g$ is

$$\bar{\theta}_{\text{opt}} = 0.558, \qquad (\bar{h}_i)_{\text{opt}} = 1.668, \qquad \text{and} \qquad n_{\text{opt}} = \frac{2\pi}{\theta_g + \dfrac{2.24(1 - \alpha_r)}{1 + \alpha_r}}$$

where $n_{\text{opt}}$ is rounded off to the nearest integer and its minimum value is 3. For *maximum stiffness*, results are identical to the above with the exception that $(\bar{h}_i)_{\text{opt}} = 1.467$. These results are obtained from Hamrock.[26]
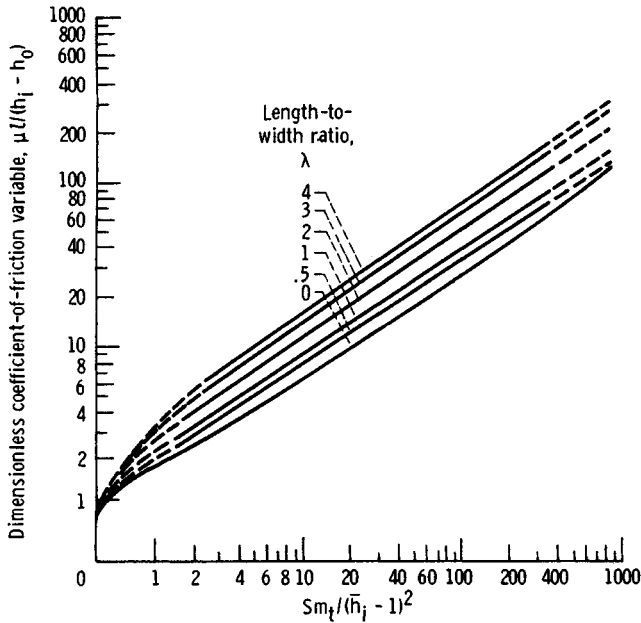
**Fig. 21.22**  Chart for determining coefficient of friction for fixed-incline pad thrust bearings. (From Ref. 25. Reprinted by permission of ASME.)
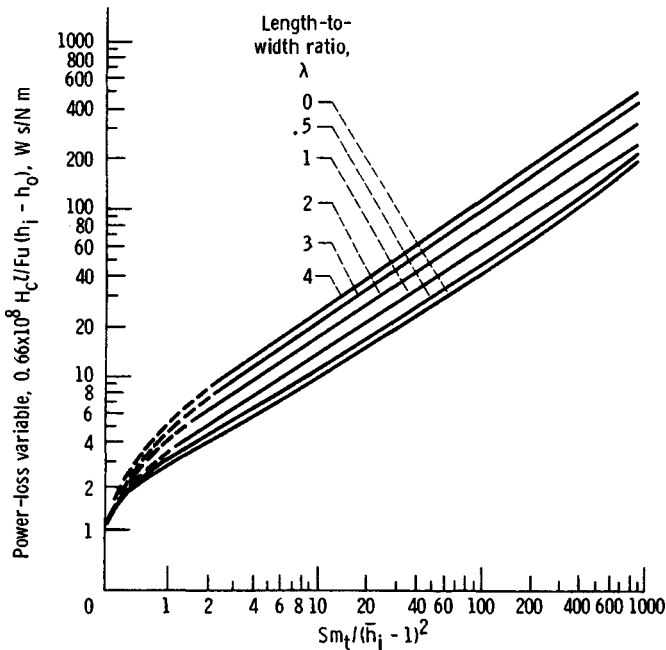


**Fig. 21.23**  Chart for determining power loss for fixed-incline pad thrust bearings. (From Ref. 25. Reprinted by permission of ASME.)
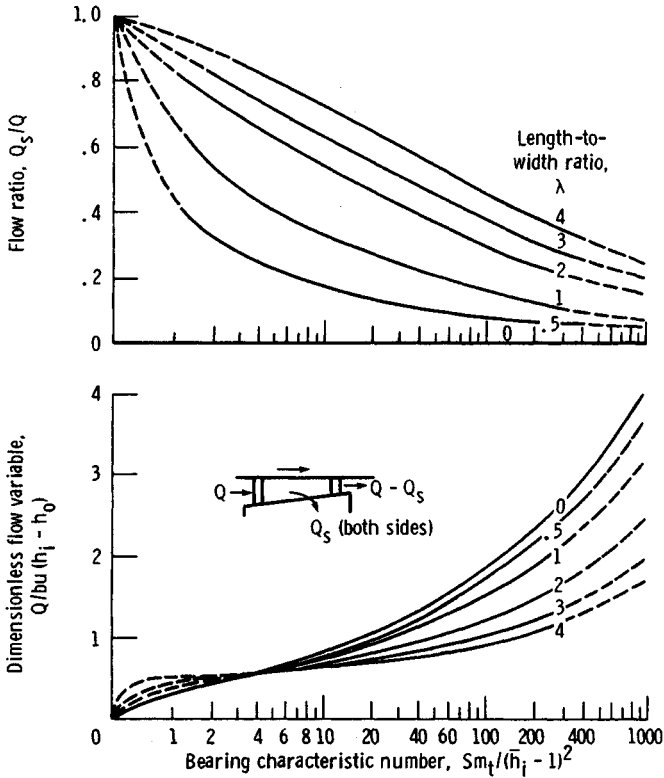
**Fig. 21.24** Charts for determining lubricant flow for fixed-incline pad thrust bearings. (From Ref. 25. Reprinted by permission of ASME.)
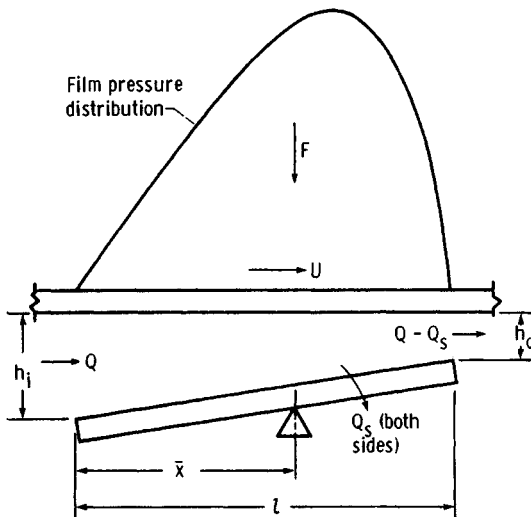


**Fig. 21.25** Configuration of pivoted-pad bearings. (From Ref. 25. Reprinted by permission of ASME.)
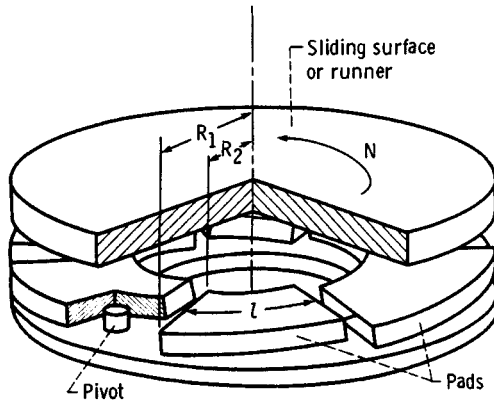
**Fig. 21.26**   Configuration of pivoted-pad thrust bearings. (From Ref. 25. Reprinted by permission of ASME.)

### 21.2.3  Hydrostatic Bearings

In Sections 21.2.1 and 21.2.2 the load-supporting fluid pressure is generated by relative motion between the bearing surfaces. Thus its load capacity depends on the relative speeds of the surfaces. When the relative speeds of the bearing are low or the loads are high, the liquid-lubricated journal and thrust bearings may not be adequate. If full-film lubrication with no metal-to-metal contact is desired under such conditions, another technique, called hydrostatic or externally pressurized lubrication, may be used.

The one salient feature that distinguishes hydrostatic from hydrodynamic bearings is that the fluid is pressurized externally to the bearings and the pressure drop across the bearing is used to support the load. The load capacity is independent of the motion of bearing surfaces or the fluid viscosity. There is no problem of contact of the surfaces at starting and stopping as with conventional hydrodynamically lubricated bearings because pressure is applied before starting and maintained until after stopping. Hydrostatic bearings can be very useful under conditions of little or no relative motion and under extreme conditions of temperature or corrosivity, where it may be necessary to use bearing materials with poor boundary lubricating properties. Surface contact can be avoided completely, so
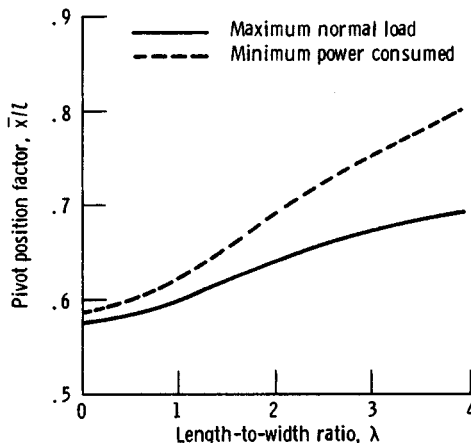


**Fig. 21.27**   Chart for determining pivot position corresponding to maximum load or minimum power loss for various pad proportions—pivoted-pad bearings. (From Ref. 25. Reprinted by permission of ASME.)
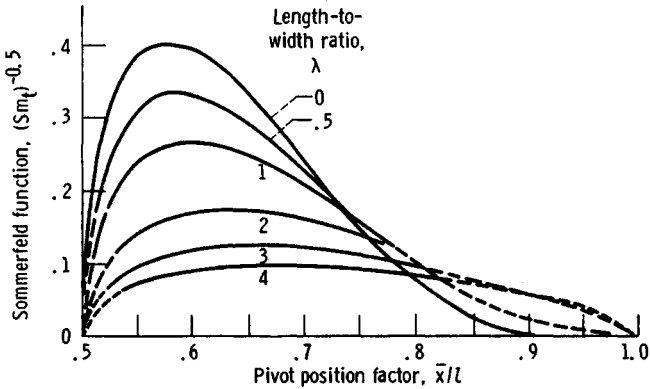
**Fig. 21.28** Chart for determining outlet film thickness for pivoted-pad thrust bearings. (From Ref. 25. Reprinted by permission of ASME.)

material properties are much less important than in hydrodynamic bearings. The load capacity of a hydrostatic bearing is proportional to the available pressure.

Hydrostatic bearings do, however, require an external source of pressurization such as a pump. This represents an additional system complication and cost.

The chief advantage of hydrostatic bearings is their ability to support extremely heavy loads at slow speeds with a minimum of driving force. For this reason they have been successfully applied in rolling mills, machine tools, radio and optical telescopes, large radar antennas, and other heavily loaded, slowly moving equipment.

The formation of a fluid film in a hydrostatic bearing system is shown in Fig. 21.34. A simple bearing system with the pressure source at zero pressure is shown in Fig. 21.34$a$. The runner under the influence of a load $F$ is seated on the bearing pad. As the source pressure builds up, Fig. 21.34$b$, the pressure in the pad recess also increases. The pressure in the recess is built up to a point, Fig. 21.34$c$, where the pressure on the runner over an area equal to the pad recess area is just sufficient to lift the load. This is commonly called the lift pressure. Just after the runner separates from the bearing pad, Fig. 21.34$d$, the pressure in the recess is less than that required to lift the bearing runner $(p_r < p_l)$. After lift, flow commences through the system. Therefore, a pressure drop exists between
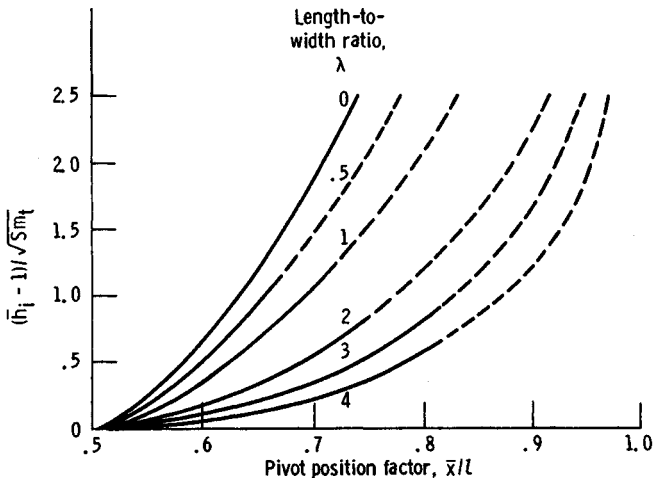


**Fig. 21.29** Chart for determining film thickness ratio $\overline{h}_i$ for pivoted-pad thrust bearings. (From Ref. 25. Reprinted by permission of ASME.)
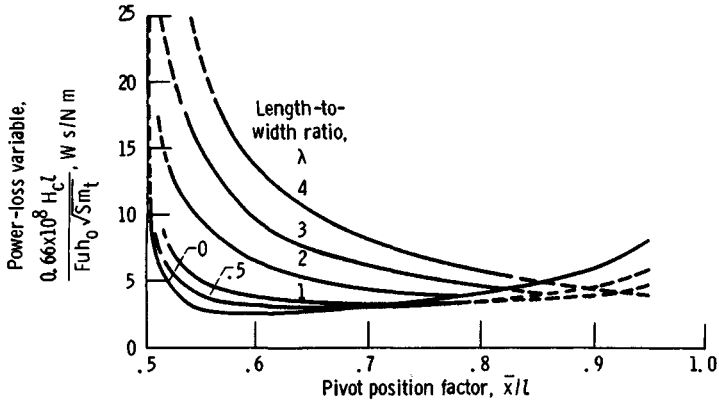
**Fig. 21.30** Chart for determining power loss for pivoted-pad thrust bearings. (From Ref. 25. Reprinted by permission of ASME.)

the pressure source and the bearing (across the restrictor) and from the recess to the exit of the bearing.

If more load is added to the bearing, Fig. 21.34e, the film thickness will decrease and the recess pressure will rise until pressure within the bearing clearance and the recess is sufficient to carry the increased load. If the load is now decreased to less than the original, Fig. 21.34f, the film thickness will increase to some higher value and the recess pressure will decrease accordingly. The maximum load that can be supported by the pad will be reached, theoretically, when the pressure in the recess is equal to the pressure at the source. If a load greater than this is applied, the bearing will seat and remain seated until the load is reduced and can again be supported by the supply pressure.

**Pad Coefficients**

To find the load-carrying capacity and flow requirements of any given hydrostatic bearing pad, it is necessary to determine certain pad coefficients. Since the selection of pad and recess geometries is up to the designer, the major design problem is the determination of particular bearing coefficients for particular geometries.

The load-carrying capacity of a bearing pad, regardless of its shape or size, can be expressed as

$$F = a_f A_p p_r \tag{21.13}$$
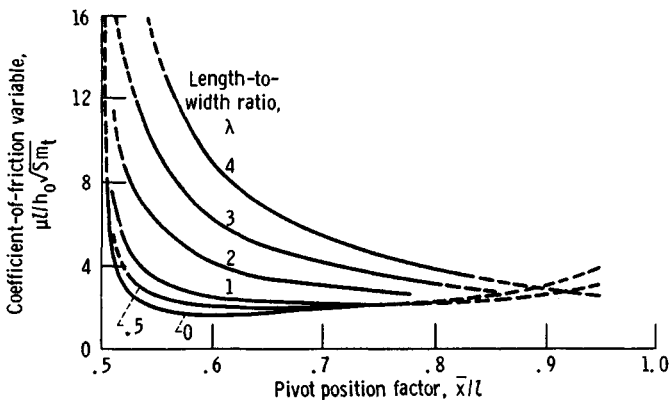
**Fig. 21.31** Chart for determining coefficient of friction for pivot-pad thrust bearings. (From Ref. 25. Reprinted by permission of ASME.)
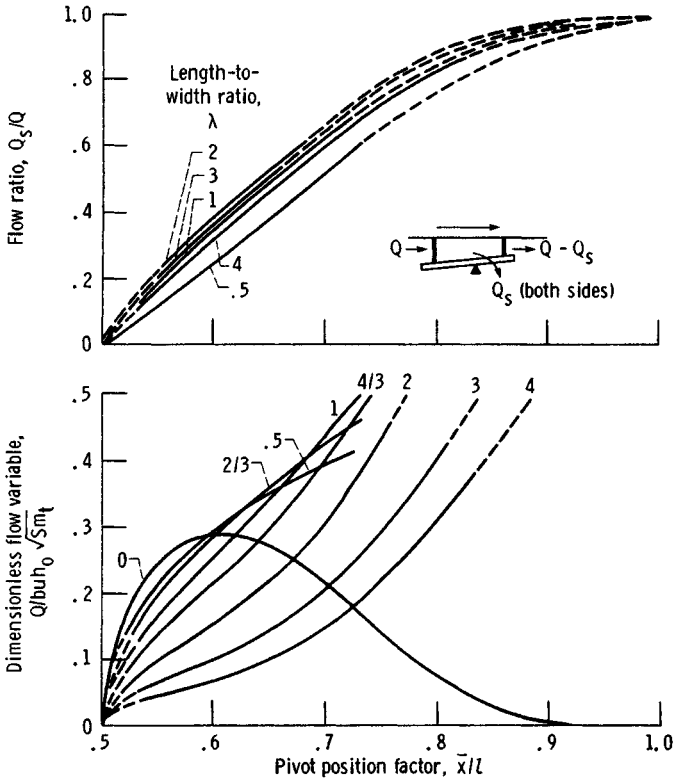
**Fig. 21.32**   Chart for determining lubricant flow for pivot-pad thrust bearings. (From Ref. 25. Reprinted by permission of ASME.)

where $a_f$ = bearing pad load coefficients
$\quad\ A_p$ = total projected pad area, m$^2$
$\quad\ p_r$ = recess pressure, N/m$^2$

The amount of lubricant flow across a pad and through the bearing clearance is

$$Q = q_f \frac{F}{A_p} \frac{h^3}{\eta} \qquad\qquad (21.14)$$

where $q_f$ = pad flow coefficient
$\quad\ h$ = film thickness, m
$\quad\ \eta$ = lubricant absolute viscosity, N sec/m$^2$

The pumping power required by the hydrostatic pad can be evaluated by determining the product of recess pressure and flow:

$$H_b = p_r Q = H_f \left(\frac{F}{A_p}\right)^2 \frac{h^3}{\eta} \qquad\qquad (21.15)$$

where $H_f = q_f/a_f$ is the bearing pad power coefficient. Therefore, in designing hydrostatic bearings the designer is primarily concerned with the bearing coefficients ($a_f$, $q_f$, and $H_f$) expressed in Eqs. (21.13)–(21.15).

Bearing coefficients are dimensionless quantities that relate performance characteristics of load, flow, and power to physical parameters. The bearing coefficients for two types of bearing pads will be considered, both of which exhibit pure radial flow and are flat, thrust-loaded types of bearings. For other types of hydrostatic bearings the reader is referred to Rippel.[22]

(a)

(b)
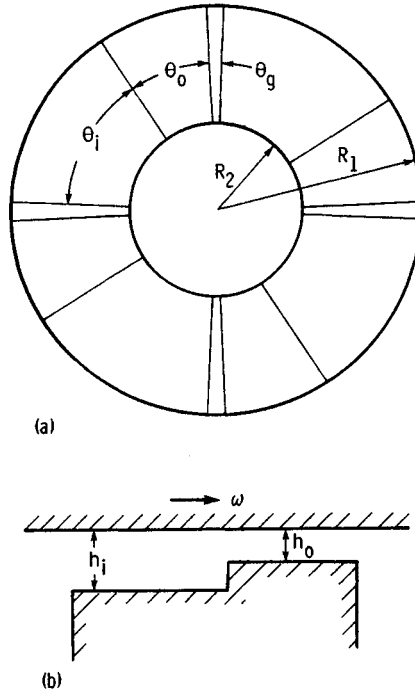
**Fig. 21.33** Configuration of step-sector thrust bearing. (From Ref. 26.) (a) Top view. (b) Section through a sector.

*Cicular Step Bearing Pad.* The bearing coefficients for this type of pad are expressed as

$$a_f = \frac{1}{2}\left[\frac{1 - (R_o/R)^2}{\log_e(R/R_o)}\right] \qquad (21.16)$$

$$q_f = \frac{\pi}{3}\left[\frac{1}{1 - (R_o/R)^2}\right] \qquad (21.17)$$

$$H_f = \frac{2\pi \log_e(R/R_o)}{3[1 - (R_o/R)^2]^2} \qquad (21.18)$$

For this type of pad the total projected bearing pad area $A_p$ is equal to $\pi R^2$.

Figure 21.35 shows the three bearing pad coefficients for various ratios of recess radius to bearing radius for a circular step thrust bearing. The bearing-pad load coefficient $a_f$ varies from zero for extremely small recesses to unity for bearings having large recesses with respect to pad dimensions. In a sense, $a_f$ is a measure of how efficiently the bearing uses the recess pressure to support the applied load.

In Fig. 21.35 we see that the pad flow coefficient $q_f$ varies from unity for pads with relatively small recesses to a value approaching infinity for bearings with extremely large recesses. Physically, as the recess becomes larger with respect to the bearing, the hydraulic resistance to fluid flow decreases, and thus flow increases.

From Fig. 21.35, the power coefficient $H_f$ approaches infinity for very small recesses, decreases to a minimum value as the recess size increases, and approaches infinity again for very large recesses. For this particular bearing the minimum value of $H_f$ occurs at a ratio of recess radius to bearing radius $R_o/R$ of 0.53. All bearing-pad configurations exhibit minimum values of $H_f$ when their ratios of recess length to bearing length are approximately 0.4 to 0.6.

*Annular Thrust Bearing.* Figure 21.36 shows an annular thrust pad bearing. In this bearing the lubricant flows from the annular recess over the inner and outer sills. For this type of bearing the pad coefficients are
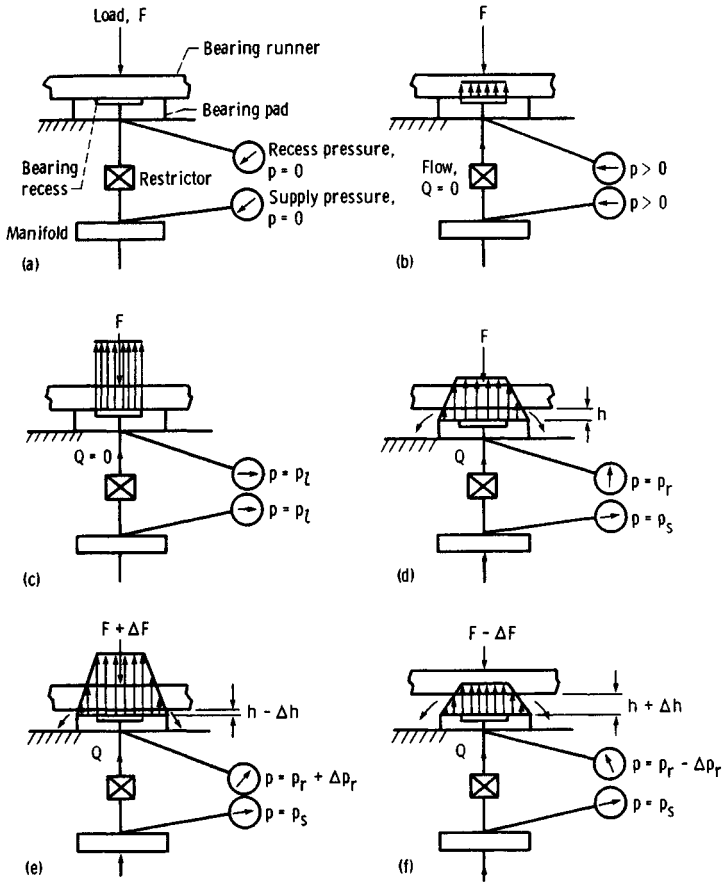
**Fig. 21.34** Formation of fluid film in hydrostatic bearing system. (From Ref. 22.) (a) Pump off. (b) Pressure building up. (c) Pressure × recess area = F. (d) Bearing operating. (e) Increased load. (f) Decreased load.

$$a_f = \frac{1}{2(R_4^2 - R_1^2)} \left[ \frac{R_4^2 - R_3^2}{\log_e(R_4/R_3)} - \frac{R_2^2 - R_1^2}{\log_e(R_2/R_1)} \right] \tag{21.19}$$

$$q_f = \frac{\pi}{6q_f} \left[ \frac{1}{\log_e(R_4/R_3)} - \frac{1}{\log_e(R_2/R_1)} \right] \tag{21.20}$$

$$H_f = \frac{q_f}{a_f} \tag{21.21}$$

For this bearing the total projected bearing-pad area is

$$A_p = \pi(R_4^2 - R_1^2) \tag{21.22}$$

Figure 21.37 shows the bearing-pad load coefficient for an annular thrust pad bearing as obtained from Eqs. (21.19)–(21.21). For this figure it is assumed that the annular recess is centrally located within the bearing width; this therefore implies that $R_1 + R_4 = R_2 + R_3$. The curve for $a_f$ applies for all $R_1/R_4$ ratios.

The hydrostatic bearings considered in this section have been limited to flat thrust-loaded bearings. Design information about other pad configurations can be obtained from Rippel.[22] The approach used for the simple, flat, thrust-loaded pad configuration is helpful in considering the more complex geometries covered by Rippel.[22]
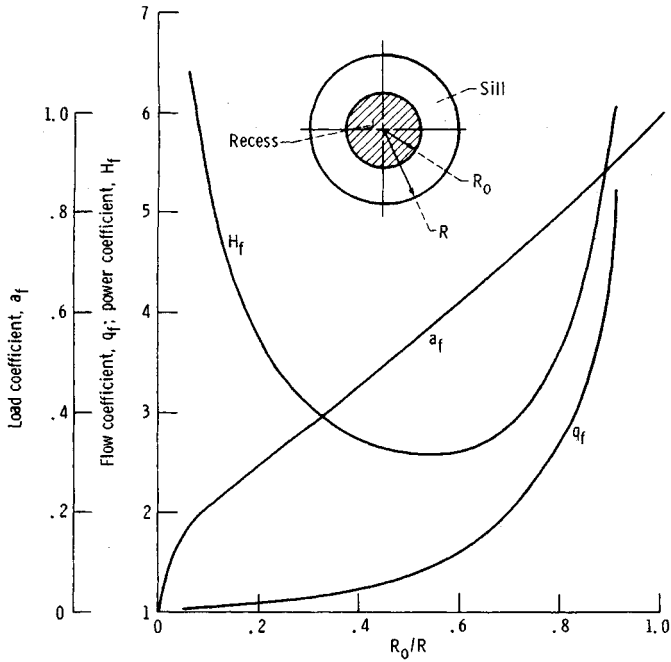
**Fig. 21.35**  Chart for determining bearing pad coefficients for circular step thrust bearing. (From Ref. 22.)
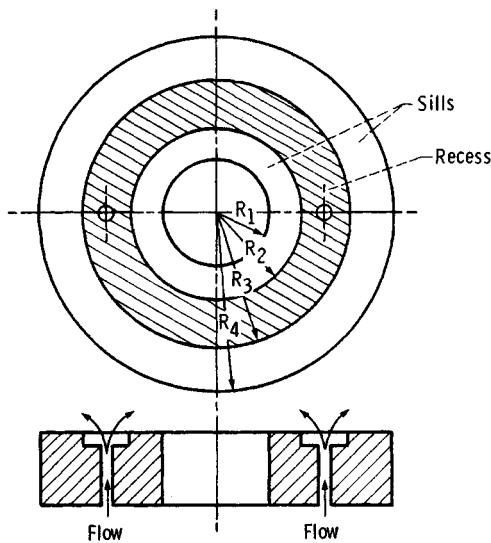


**Fig. 21.36**  Configuration of annular thrust pad bearing. (From Ref. 22.)
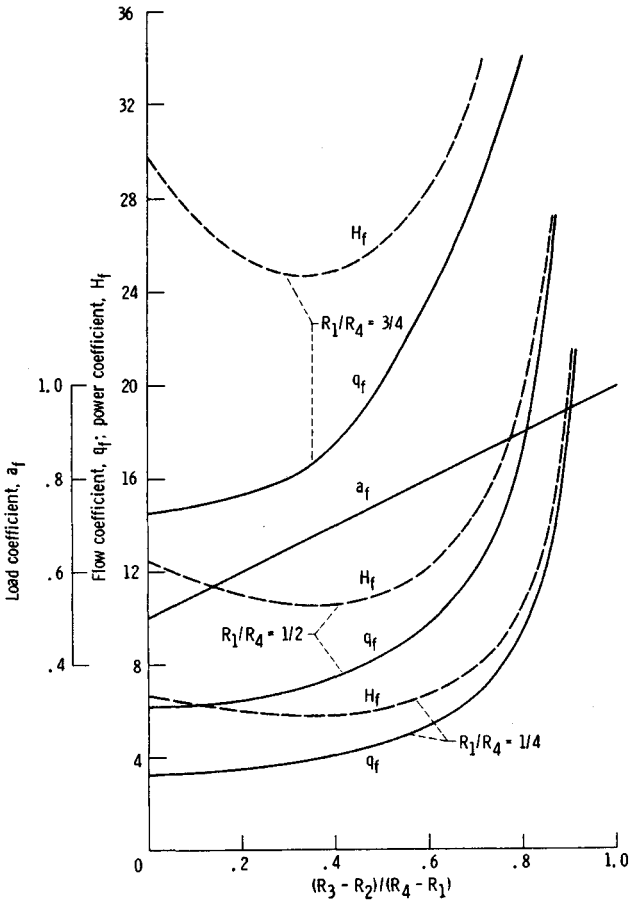
**Fig. 21.37** Chart for determining bearing pad coefficients for annular thrust pad bearings. (From Ref. 22.)

## Compensating Elements

As compared with common bearing types, hydrostatic bearings are relatively complex systems. In addition to the bearing pad, the system includes a pump and compensating elements. Three common types of compensating elements for hydrostatic bearings are the capillary tube, the sharp-edged orifice, and constant-flow-valve compensation.

*Capillary Compensation.* Figure 21.38 shows a capillary-compensated hydrostatic bearing as obtained from Rippel.[22] The small diameter of the capillary tube provides restriction and resultant pressure drop in the bearing pad. The characteristic feature of capillary compensation is a long tube or a relatively small diameter ($l_c > 20d_c$). The laminar flow of fluid through such a tube while neglecting entrance and exit effects and viscosity changes due to temperature and pressure effects can be expressed as

$$Q_c = \frac{k_c(p_s - p_r)}{\eta} \tag{21.23}$$

where

$$k_c = \frac{\pi d_c^4}{128 l_c} \tag{21.24}$$
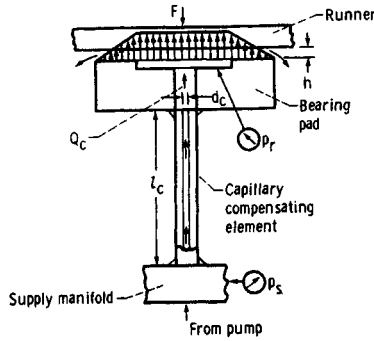
**Fig. 21.38**  Capillary-compensated hydrostatic bearing. (From Ref. 22.)

For a given capillary tube, $k_c$ is a constant expressed in cubic meters. Thus, from Eq. (21.23) the flow through a capillary tube is related linearly to the pressure drop across it. In a hydrostatic bearing with capillary compensation and a fixed supply pressure, the flow through the bearing will decrease with increasing load since the pocket pressure $p_r$ is proportional to the load. To satisfy the assumption of laminar flow, Reynolds number must be less than 2000 when expressed as

$$N_R = \frac{4\rho Q_c}{\pi d_c \eta} < 2000 \qquad (21.25)$$

where $\rho$ is the mass density of the lubricant in N sec$^2$/m$^4$. Hypodermic needle tubing serves quite well as capillary tubing for hydrostatic bearings. Although very small diameter tubing is available, diameters less than $6 \times 10^{-4}$ m should not be used because of their tendency to clog.

***Orifice Compensation.***   Orifice compensation is illustrated in Fig. 21.39. The flow of an incompressible fluid through a sharp-edged orifice can be expressed as

$$Q_o = k_o(p_s - p_r)^{1/2} \qquad (21.26)$$

where

$$k_o = \frac{\pi c_a d_o^2}{\sqrt{8\rho}}$$

and $c_d$ is the orifice discharge coefficient. For a given orifice size and given lubricant, $k_o$ is a constant
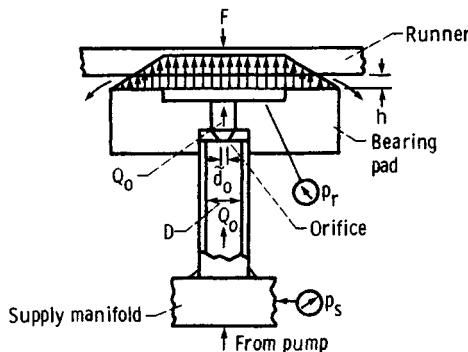


**Fig. 21.39**  Orifice-compensated hydrostatic bearing. (From Ref. 22.)

expressed in $\text{m}^4/\text{sec N}^{1/2}$. Thus, from Eq. (21.26) flow through an orifice is proportional to the square root of the pressure difference across the orifice.

The discharge coefficient $c_d$ is a function of Reynolds number. For an orifice the Reynolds number is

$$N_R = \frac{d_o}{\eta}\,[2\rho(p_s - p_r)]^{1/2} \tag{21.27}$$

For a Reynolds number greater than approximately 15, which is the usual case in orifice-compensated hydrostatic bearings, $c_d$ is about 0.6 for $d_o/D < 0.1$. For a Reynolds number less than 15, the discharge coefficient is approximately

$$c_d = 0.20\sqrt{N_R} \tag{21.28}$$

The pipe diameter $D$ at the orifice should be at least 10 times the orifice diameter $d_o$. Sharp-edged orifices, depending on their diameters, have a tendency to clog, therefore orifice diameters $d_o$ less than $5 \times 10^{-4}$ m should be avoided.

*Constant-Flow-Valve Compensation.* Constant-flow-valve compensation is illustrated in Fig. 21.40. This type of restrictor has a constant flow regardless of the pressure difference across the valve. Hence, the flow is independent of recess pressure.

The relative ranking of the three types of compensating elements with regard to a number of considerations is given in Table 21.6. A rating of 1 in this table indicates best or most desirable. This table should help in deciding which type of compensation is most desirable in a particular application.

Basically, any type of compensating element can be designed into a hydrostatic bearing system if loads on the bearing never change. But if stiffness, load, or flow vary, the choice of the proper compensating element becomes more difficult and the reader is again referred to Rippel.[22]

### 21.2.4 Gas-Lubricated Hydrodynamic Bearings

A relatively recent (within the last 30 years) extension of hydrodynamic lubrication that is of growing importance is gas lubrication. It consists of using air or some other gas as a lubricant rather than a mineral oil. The viscosity of air is 1000 times smaller than that of very thin mineral oils. Consequently, the viscous resistance is very much less. However, the distance of nearest approach (i.e., the closest distance between the shaft and the bearing) is also correspondingly smaller, so that special precautions must be taken. To obtain full benefits from gas lubrication, the following should be observed:

1. Surfaces must have a very fine finish.
2. Alignment must be very good.
3. Dimensions and clearances must be very accurate.
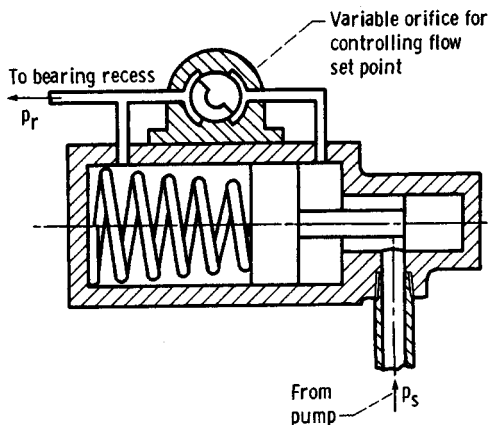


**Fig. 21.40**   Constant-flow-valve compensation in hydrostatic bearing. (From Ref. 22.)

**Table 21.6   Compensating-Element Considerations[a] (From Ref. 22)**

| Consideration | Capillary | Orifice | Constant-flow Valve |
|---|---|---|---|
| | Compensating Element | | |
| Initial cost | 2 | 1 | 3 |
| Cost to fabricate and install | 2 | 3 | 1 |
| Space required | 2 | 1 | 3 |
| Reliability | 1 | 2 | 3 |
| Useful life | 1 | 2 | 3 |
| Commercial availability | 2 | 3 | 1 |
| Tendency to clog | 1 | 2 | 3 |
| Serviceability | 2 | 1 | 3 |
| Adjustability | 3 | 2 | 1 |

[a]Rating of 1 is best or most desirable.

4.  Speeds must be high.
5.  Loading must be relatively low.

Another main difference between the behavior of similar gas and liquid films besides that of viscosity is the compressibility of the gas. At low relative speeds it is reasonable to expect the gas-film density to remain nearly constant and the film therefore to behave as if it were incompressible. At high speeds, however, the density change is likely to become of primary importance so that such gas-film properties must differ appreciably from those of similar liquid films.

Gas-lubricated bearings can also operate at very high temperatures since the lubricant will not degrade chemically. Furthermore, if air is used as the lubricant, it costs nothing. Gas bearings are finding increasing use in gas-cycle machinery where the cycle gas is used in the bearings, thus eliminating the need for a conventional lubrication system; in gyros, where precision and constancy of torque are critical; in food and textile processing machinery, where cleanliness and absence of contaminants are critical; and also in the magnetic recording tape industry.

**Journal Bearings**

Plain gas-lubricated journal bearings are of little interest because of their poor stability characteristics. Lightly loaded bearings that operate at low eccentricity ratios are subjected to fractional frequency whirl, which can result in bearing destruction. Two types of gas-lubricated journal bearings find widespread use, namely, the pivoted pad and the herringbone groove.

*Pivoted Pad.*   Pivoted-pad journal bearings are most frequently used as shaft supports in gas-bearing machinery because of their excellent stability characteristics. An individual pivot pad and shaft are shown in Fig. 21.41, and a three-pad pivoted-pad bearing assembly is shown in Fig. 21.42. Generally, each pad provides pad rotation degrees of freedom about three orthogonal axes (pitch, roll, and yaw). Pivoted-pad bearings are complex because of the many geometric variables involved in their design. Some of these variables are:

1.  Number of pads.
2.  Circumferential extent of pads, $\alpha_p$.
3.  Aspect ratio of pad, $R/l$.
4.  Pivot location, $\phi_p/\alpha_p$.
5.  Machined-in clearance ratio, $c/R$.
6.  Pivot circle clearance ratio, $c'/R$.
7.  Angle between line of centers and pad leading edge, $\xi_p$.

Analysis is accomplished by first determining the characteristics of an individual pad. Both geometric and operating parameters influence the design of a pivoted pad. The operating parameter of importance is the dimensionless bearing number $\Lambda_j$, where

$$\Lambda_j = \frac{6\eta\omega R^2}{p_a c^2}$$
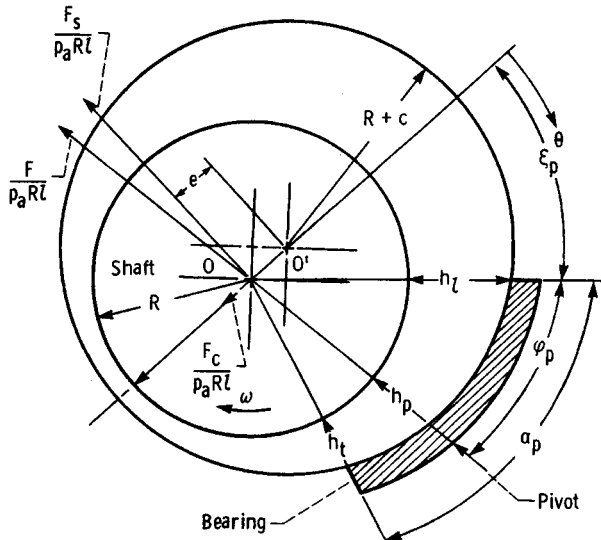
**Fig. 21.41** Geometry of individual shoe-shaft bearing. (From Ref. 27.)
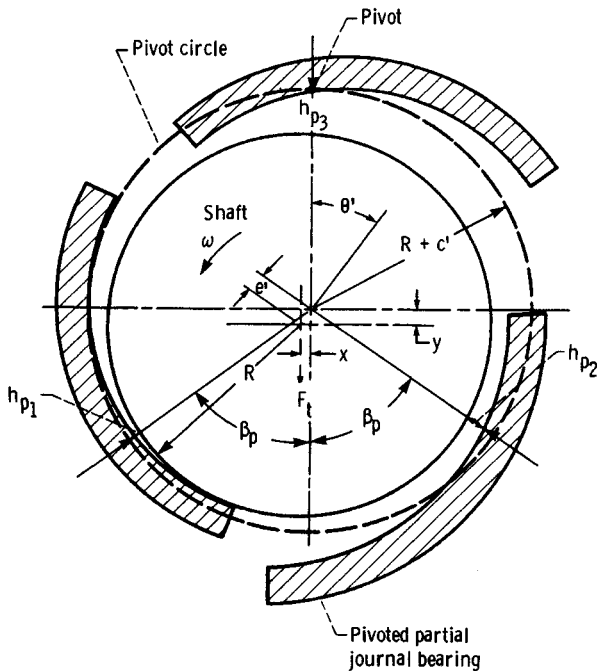


**Fig. 21.42** Geometry of pivoted-pad journal bearing with three shoes. (From Ref. 27.)

The results of computer solutions obtained from Gunter et al.[27] for the performance of a single pad are shown in Figs. 21.43–21.45. These figures illustrate load coefficient, pivot film thickness, and trailing-edge film thickness as functions of pivot location and eccentricity ratio. These field maps apply for a pad with a radius-to-width ratio of 0.606, a circumferential extent of 94.5° (an aspect ratio of 1), and $\Lambda_j = 3.5$. For other geometries and $\Lambda$ values similar maps must be generated. Additional maps are given in Gunter et al.[27]

Figures 21.46–21.48 show load coefficient and stiffness coefficient for a range of $\Lambda_j$ values up to 4. These plots are for a pivot position of $\frac{2}{3}$.

When the individual pad characteristics are known, the characteristics of the multipad bearing can be determined by using a trial-and-error approach. With the arrangement shown in Fig. 21.42, the load is directed between the two lower pivots. For this case the load carried by each of the lower pads is initially assumed to be $F \cos \beta$. The pivot film thicknesses $h_{p_1}$ and $h_{p_2}$ are then calculated. The upper-pad pivot film thickness $h_{p_3}$, eccentricity ratio $\epsilon$, and load coefficient $C_{l_3}$ can be determined. The additional load on the shaft due to the reaction of pad 3 is added to the system load. Calculations are repeated until the desired accuracy is achieved.

Pivoted-pad journal bearings are usually assembled with a pivot circle clearance $c'$ somewhat less than the machined-in clearance $c$. When $c'/c < 1$, the bearing is said to be preloaded. Preload is usually given in terms of a preload coefficient, which is equal to $(c - c')/c$. Preloading is used to increase bearing stiffness and to prevent complete unloading of one or more pads. The latter condition can lead to pad flutter and possible contact of the pad leading edge and the shaft, which, in turn, can result in bearing failure.

***Herringbone Groove.***   A fixed-geometry bearing that has demonstrated good stability characteristics and thus promise for use in high-speed gas bearings is the herringbone bearing. It consists of a circular journal and bearing sleeve with shallow, herringbone-shaped grooves cut into either member. Figure 21.49 illustrates a partially grooved herringbone journal bearing. In this figure the groove and bearing parameters are also indicated. Figures 21.50–21.54 were obtained from Hamrock and Fleming[28] and are design charts that present curves for optimizing the design parameters for herringbone journal bearings for maximum radial load. The (*a*) portion of these figures is for the grooved member rotating and the (*b*) portion is for the smooth member rotating. The only groove parameter not represented in these figures is the number of grooves to be used. From Hamrock and Fleming[28] it was found that the *minimum* number of grooves to be placed around the journal can be represented by $n \geq \Lambda_j/5$.

More than any other factors, self-excited whirl instability and low-load capacity limit the usefulness of gas-lubricated journal bearings. The whirl problem is the tendency of the journal center to orbit the bearing center at an angular speed less than or equal to half that of the journal about its own center. In many cases the whirl amplitude is large enough to cause destructive contact of the bearing surfaces.

Figure 21.55, obtained from Fleming and Hamrock,[29] shows the stability attained by the optimized herringbone bearings. In this figure the stability parameter $\overline{M}$ is introduced, where

$$\overline{M} = \frac{\overline{m} p_a h_r^5}{2R^5 l \eta^2}$$

and $\overline{m}$ is the mass supported by the bearing.

In Fig. 21.55, the bearings with the grooved member rotating are substantially more stable than those with the smooth member rotating, especially at high compressibility numbers.

### Thrust Bearings

Two types of gas-lubricated thrust bearings have found the widest use in practical applications. These are the Rayleigh step and the spiral- or herringbone-groove bearings.

***Rayleigh Step Bearing.***   Figure 21.56 shows a Rayleigh step thrust bearing. In this figure the ridge region is where the film thickness is $h_r$ and the step region is where the film thickness is $h_s$. The feed groove is the deep groove separating the end of the ridge region and the beginning of the next step region. Although not shown in the figure, the feed groove is orders of magnitude deeper than the film thickness $h_r$. A pad is defined as the section that includes ridge, step, and feed groove regions. The length of the feed groove is small relative to the length of the pad. It should be noted that each pad acts independently since the pressure profile is broken at the lubrication feed groove.

The load capacity and stiffness of a Rayleigh step thrust bearing are functions of the following parameters:

1.  $\Lambda_t = 6 \eta u l / p_a h_r^2$, the dimensionless bearing number.
2.  $\lambda_a = (b_r + b_s + b_g)/l$, length ratio.
3.  $H_a = h_s / h_r$, film thickness ratio.
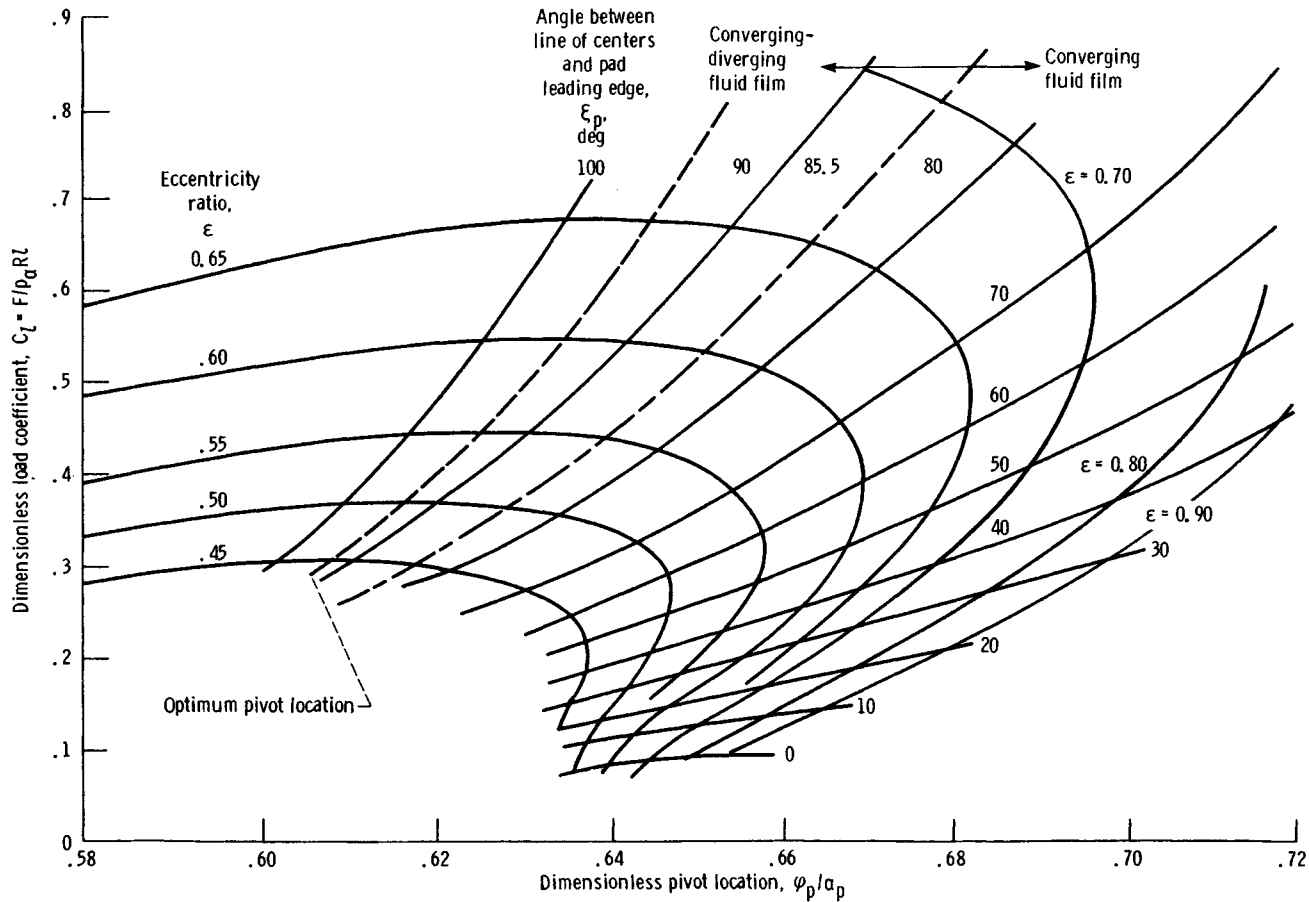
**Fig. 21.43** Chart for determining load coefficient. Bearing radius-to-length ratio, $R/l$, 0.6061; angular extent of pad, $\alpha_p$, 94.5°; dimensionless bearing number, $A_j$, 3.5. (From Ref. 27.)
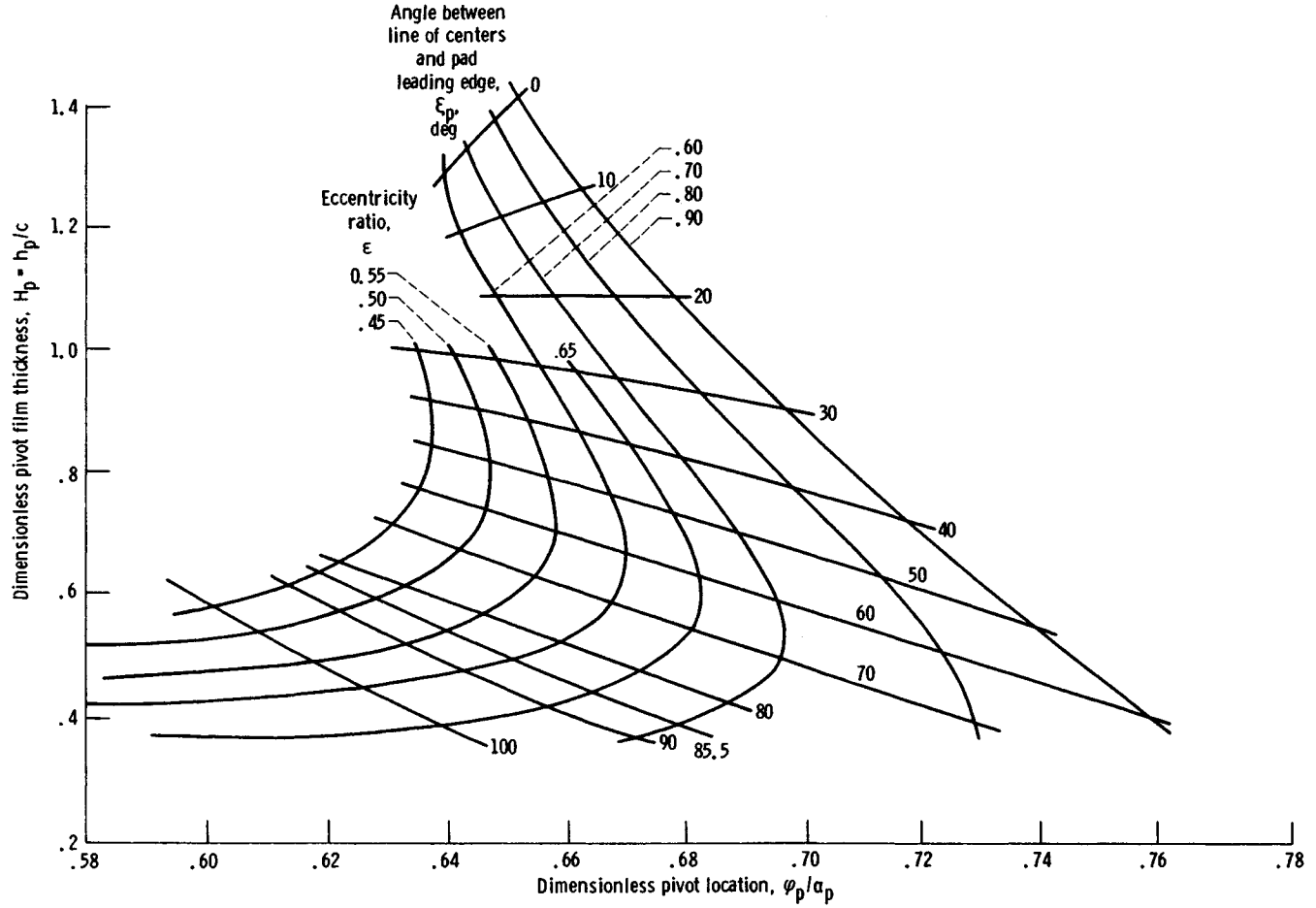
**Fig. 21.44** Chart for determining pivot film thickness. Bearing radius-to-length ratio, $R/l$, 0.6061; angular extent of pad, $\alpha_p$, 94.5°; dimensionless bearing number, $A_j$, 3.5. (From Ref. 27.)
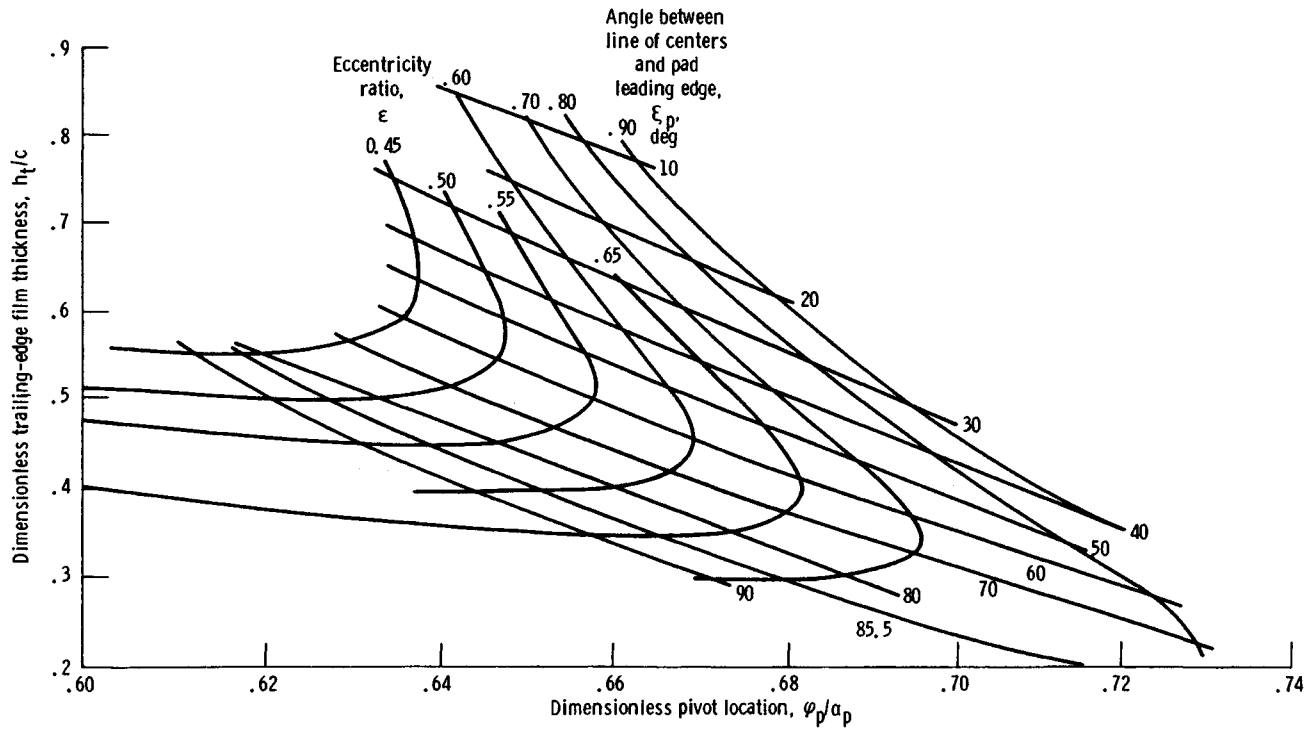
**Fig. 21.45** Chart for determining trailing-edge film thickness. Bearing radius-to-length ratio, $R/l$, 0.6061; angular extent of pad, $\alpha_p$, 94.5°, dimensionless bearing number, $A_j$, 3.5. (From Ref. 27.)
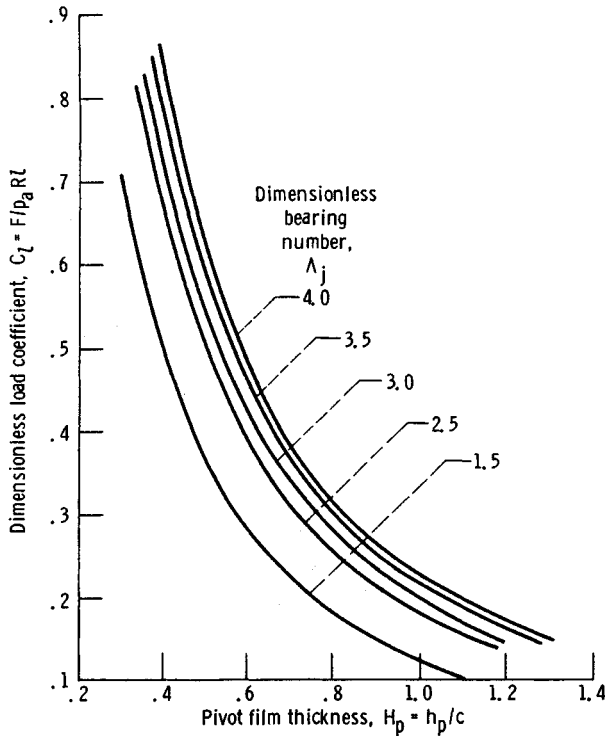
**Fig. 21.46** Chart for determining load coefficient. Angular extent of pad, $\alpha_p$, 94.5°; ratio of angle between pad leading edge and pivot to $\alpha_p$, $\varphi_p/\alpha_p$, $\frac{2}{3}$; length-to-width ratio, $\lambda$, 1.0. (From Ref. 27.)

4.  $\psi_s = b_s/(b_s + b_r + b_g)$, step location parameter.

Figure 21.57a shows the effect of $\Lambda_t$ on $\lambda_a$, $H_a$, and $\psi_s$ for the *maximum-load-capacity condition*. The optimal step parameters $\Lambda_a$, $H_a$, and $\psi_s$ approach an asymptote as the dimensionless bearing number $\Lambda_t$ becomes small. This asymptotic condition corresponds to the incompressible solution or $\lambda_a = 0.918$, $\psi_s = 0.555$, $H_a = 1.693$. For $\Lambda_t > 1$ it is observed that there is a different optimum value of $\lambda_a$, $H_a$, and $\psi_s$ for each value of $\Lambda_t$.

Figure 21.57b shows the effect of $\Lambda_t$ on $\lambda_a$, $H_a$, and $\psi_s$ for the *maximum-stiffness condition*. As in Fig. 21.57a the optimal step parameters approach asymptotes as the incompressible solution is reached. The asymptotes are $\lambda_a = 0.915$, $\psi_s = 0.557$, and $H_a = 1.470$. Note that there is a difference in the asymptote for the film thickness ratio but virtually no change in $\lambda_a$ and $\psi_s$ when compared with the results obtained for maximum-load-capacity condition.

Figure 21.58 shows the effect of dimensionless bearing number $\Lambda_t$ on dimensionless load capacity and stiffness. The difference in these figures is that the optimal step parameters are obtained in Fig. 21.58a for maximum load capacity and in Fig. 21.58b for maximum stiffness.

For optimization of a step-sector thrust bearing, parameters for the sector must be found that are analogous to those for the rectangular step bearing. The following substitutions accomplish this transformation:

$$l \rightarrow R_1 - R_2$$
$$n(b_s + b_r + b_g) \rightarrow \pi(R_1 + R_2)$$
$$u \rightarrow \frac{\omega}{2}(R_1 + R_2)$$

where $n$ is the number of pads placed in the step sector. By making use of these equations, the dimensionless bearing number can be rewritten as
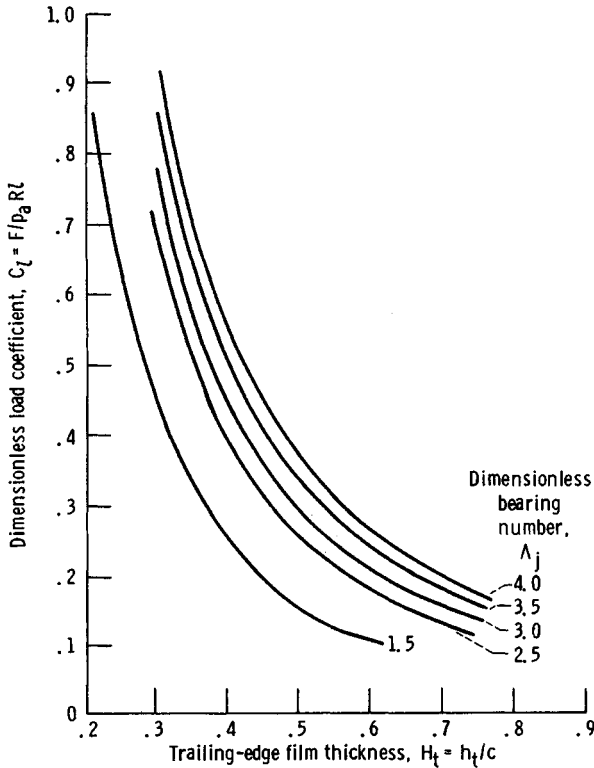
**Fig. 21.47**  Chart for determining load coefficient. Angular extent of pad, $\alpha_p$, 94.5°; ratio of angle between pad loading edge and pivot to $\alpha_p$, $\varphi_p/\alpha_p$, $\frac{2}{3}$; length-to-width ratio, $\lambda$, 1.0. (From Ref. 27.)

$$\Lambda_c = \frac{3\eta\omega(R_1^2 - R_2^2)}{p_a h_r^2}$$

The optimal number of pads to be placed in the sector is obtained from the formula

$$n = \frac{\pi(R_1 + R_2)}{(\lambda_a)_{\text{opt}}(R_1 - R_2)}$$

where $(\lambda_a)_{\text{opt}}$ is obtained from Fig. 21.57a or 21.57b for a given dimensionless bearing number $\Lambda_t$. Since $n$ will not normally be an integer, rounding it to the nearest integer is required. Therefore, through the parameter transformation discussed above, the results presented in Figs. 21.57 and 21.58 are directly usable in designing optimal step-sector gas-lubricated thrust bearings.

*Spiral-Groove Thrust Bearings.*  An inward-pumping spiral-groove thrust bearing is shown in Fig. 21.59. An inward-pumping thrust bearing is somewhat more efficient than an outward-pumping thrust bearing and therefore is the only type considered here.

The dimensionless parameters normally associated with a spiral-groove thrust bearing are:

1. Angle of inclination, $\beta_a$.
2. Width ratio, $\bar{b} = b_s/b_r$.
3. Film ratio, $H_a = h_s/h_r$.
4. Radius ratio, $\alpha_r = R_2/R_1$.
5. Groove length fraction, $\bar{R} = (R_1 - R_g)/(R_1 - R_2)$.
6. Number of grooves, $n$.
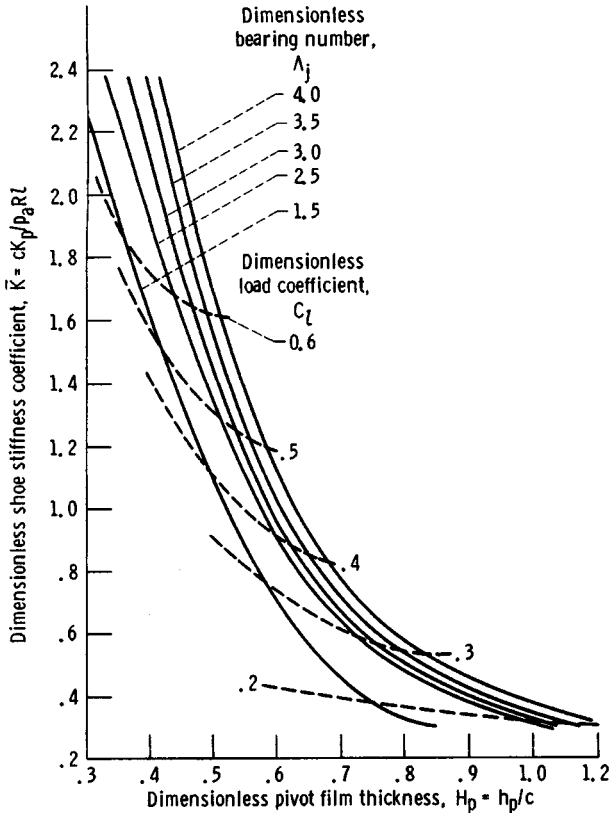
**Fig. 21.48**  Chart for determining shoe stiffness coefficient. (From Ref. 27.)

7.  Dimensionless bearing number, $\Lambda_c = 3\eta\omega(R_1^2 - R_2^2)/p_a h_r^2$.

The first six parameters are geometrical parameters and the last parameter is an operating parameter.
    The performance of spiral-groove thrust bearings is represented by the following dimensionless parameters:
    *Load*

$$\overline{W}_\infty = \frac{1.5 G_f F}{\pi p_a (R_1^2 - R_2^2)} \tag{21.29}$$

*Stiffness*

$$\overline{K}_\infty = \frac{1.5 h_r G_f K_p}{\pi p_a (R_1^2 - R_2^2)} \tag{21.30}$$

*Flow*

$$\overline{Q} = \frac{3\eta Q}{\pi p_a h_r^3} \tag{21.31}$$

*Torque*

$$\overline{T} = \frac{6 T_r}{\pi p_a (R_1^2 + R_2^2) h_r \Lambda_c} \tag{21.32}$$

When the geometrical and operating parameters are specified, the load, stiffness, flow, and torsion can be obtained.
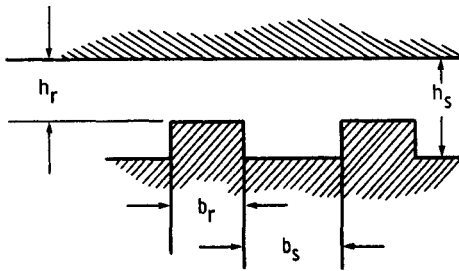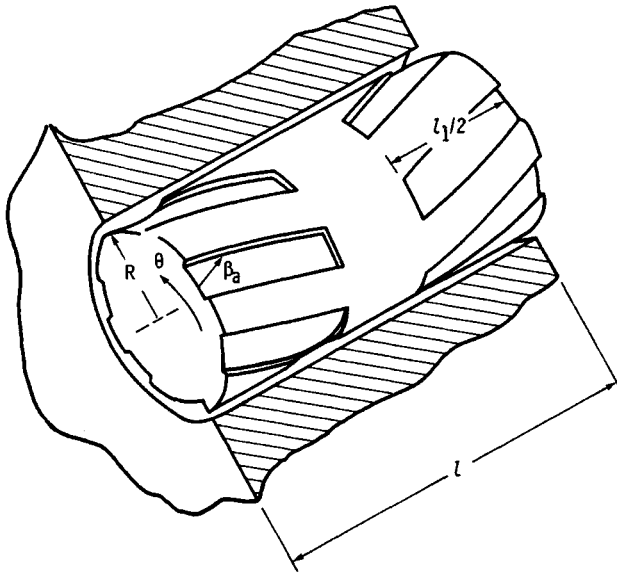
**Fig. 21.49**  Configuration of concentric herringbone-groove journal bearing. Bearing parameters; $\lambda = l/2R$; $\Lambda_j = 6\mu UR/p_a h_r^2$. Groove parameters; $H_a = h_s/h_r$; $\alpha_b = b_s/(b_r + b_s)$; $\beta_a$, $\gamma = l_1/l$; $n$. (From Ref. 28.)

The design charts of Reiger[20] are reproduced as Figs. 21.60–21.66. Figure 21.60 shows the dimensionless load for various radius ratios as a function of dimensionless bearing number $\Lambda_c$. This figure can be used to calculate the dimensionless load for a finite number of grooves; Fig. 21.61 can be used to determine the value of the groove factor. Figure 21.62 shows curves of dimensionless stiffness; Fig. 21.63 shows curves of dimensionless flow; and Fig. 21.64 shows curves of dimensionless torque. Optimized groove geometry parameters can be obtained from Fig. 21.65. Finally, Fig. 21.66 is used to calculate groove radius $R_g$ (shown in Fig. 21.59). Figure 21.66 shows the required groove length fraction $\overline{R} = (R_o - R_g)/(R_o - R_i)$ to ensure stability from self-excited oscillations.

In a typical design problem the given factors are load, speed, bearing envelope, gas viscosity, ambient pressure, and an allowable radius-to-clearance ratio. The maximum value of the radius-to-clearance ratio is usually dictated by the distortion likely to occur to the bearing surfaces. Typical values are 5000–10,000. The procedure normally followed in designing a spiral-groove thrust bearing while using the design curves given in Figs. 21.60–21.66 is as follows:

1. Select the number of grooves $n$.
2. From Fig. 21.61 determine the groove factor $G_f$ for given $\alpha_r = R_i/R_o$ and $n$.
3. Calculate $\overline{W}_\infty = 1.5 G_f F/\pi p_a(R_1^2 - R_2^2)$.
4. If $\overline{W}_\infty < 0.8$, $R_1$ must be increased. Return to step 2.
5. From Fig. 21.60, given $\overline{W}_\infty$ and $\alpha_r$ establish $\Lambda_c$.
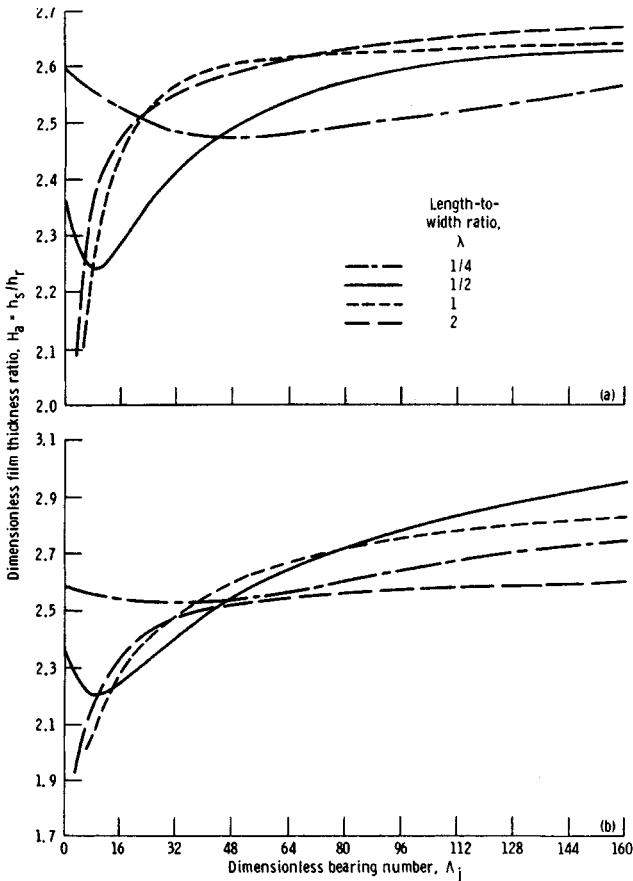
**Fig. 21.50** Chart for determining optimal film thickness. (From Ref. 28.) (a) Grooved member rotating. (b) Smooth member rotating.

6. Calculate

$$\frac{R_1}{h_r} = \left\{ \frac{\Lambda_c p_a}{3\eta(\omega_h - \omega_o)[1 - (R_2/R_1)^2]} \right\}^{1/2}$$

If $R_1/h_r > 10,000$ (or whatever preassigned radius-to-clearance ratio), a larger bearing or higher speed is required. Return to step 2. If these changes cannot be made, an externally pressurized bearing must be used.

7. Having established what $\alpha_r$ and $\Lambda_c$ should be, obtain values of $\overline{K}_\infty$, $\overline{Q}$, and $\overline{T}$ from Figs. 21.62, 21.63, and 21.64, respectively. From Eqs. (21.29), (21.30), and (21.31) calculate $K_p$, $Q$, and $T_r$.

8. From Fig. 21.65 obtain groove geometry ($b$, $\beta_a$, and $H_a$) and from Fig. 21.66 obtain $R_g$.

## 21.3 ELASTOHYDRODYNAMIC LUBRICATION

Downson[31] defines elastohydrodynamic lubrication (EHL) as "the study of situations in which elastic deformation of the surrounding solids plays a significant role in the hydrodynamic lubrication process." Elastohydrodynamic lubrication implies complete fluid-film lubrication and no asperity interaction of the surfaces. There are two distinct forms of elastohydrodynamic lubrication.

1. *Hard EHL.* Hard EHL relates to materials of high elastic modulus, such as metals. In this form of lubrication not only are the elastic deformation effects important, but the pressure–viscosity